 doi:10.20944/preprints202106.0059.v1

Design and Applications of Multi-Frequency Holographic Subsurface Radar: Review and Case Histories

Sergey Ivashov[1], Lorenzo Capineri[2], Timothy Bechtel[3], Vladimir Razevig[1], Masaharu Inagaki[4], Nikolay Litchkov[5], and Ahmet Kizilay[6]

1 – Remote Sensing Laboratory, Bauman Moscow State Technical University, Russia
sivashov@rslab.ru , vrazevig@rslab.ru
2 – Department of Information Engineering, University of Florence, Italy,
lorenzo.capineri@unifi.it
3 – Department of Earth & Environment, Franklin & Marshall College, PA, USA,
timothy.bechtel@fandm.edu
4 – Walnut Ltd., Tokyo, Japan, ina_mas@beige.plala.or.jp
5 – Bulgarian Academy of Sciences – IMSET, Bulgaria, niki0611@abv.bg
6 – Electronics and Communications Engineering Department, Yildiz Technical University, Turkey, akizilay@yildiz.edu.tr

Corresponding author: Lorenzo Capineri lorenzo.capineri@unifi.it

Abstract: Holographic subsurface radar (HSR) is currently not in widespread usage. This is due to an historical perspective in the ground penetrating radar (GPR) community that the high attenuation of electromagnetic waves in most media of interest, and the inability to apply time-varying gain to the continuous wave (CW) HSR signal precludes sufficient effective penetration depth. While it is true that the fundamental physics of HSR, with its use of a CW signal, does not allow amplification of later (i.e. deeper) arrivals in lossy media (as is possible with impulse subsurface radar — ISR), HSR has distinct advantages. The most important of these is the ability to do shallow subsurface imaging with a resolution that is not possible with ISR. In addition, the design of an HSR system is simpler than for ISR due to the relatively low-tech transmitting and receiving antennae. This paper provides a review of the main principles of HSR through an optical analogy and describes possible algorithms for radar hologram reconstruction. We also present a review of the history of development of systems and applications for HSR of the "RASCAN" type which is possibly the only commercially available holographic subsurface radars. Among the subsurface imaging and remote sensing applications considered are humanitarian demining, construction inspection, surveys of historic architecture and artworks, nondestructive testing of dielectric aerospace materials, security applications, paleontology, detection of wood-boring insect damage, and others. Each application is illustrated with relevant data acquired in laboratory and/or field experiments.

Keywords: Holographic subsurface radar, ground penetrating radar, nondestructive testing, cultural heritage objects, humanitarian demining, human vital signals monitoring, security applications.

1. Introduction

In the early days of their development (1970s and early 1980s), subsurface radars were primarily developed as an electromagnetic technique for detection of subsurface objects at depths of up to a few meters below ground surface [1], [2], [3]. This was dictated by the typical operational frequency range of 100 MHz to 500 MHz, which was achievable with impulse subsurface radar at that time. Depth resolution in this band was limited to 0.5 m to 1 m, and the main media under consideration at that time were soils and fresh water ice [3]. It was these

Preprints (www.preprints.org) | NOT PEER-REVIEWED | Posted: 2 June 2021 doi:10.20944/preprints202106.0059.v1

applications that gave the name Ground Penetrating Radar and its acronym (GPR) to this early type of radar. This acronym is still in wide use despite the fact that modern subsurface radars have much wider areas of application, deserving of the more accurate name of surface-penetrating radar [2] or subsurface interface radar (SIR) [4].

All types of GPR can be divided into three categories by the characteristics of the emitted signal:

- Time-domain impulse radars
- Frequency-modulated continuous-wave radars
- Holographic radars.

This classification, as adapted from [2], is presented in Fig. 1. The last type of subsurface radar — holographic subsurface radar (HSR) is the topic of this review. It is important to note at the outset that HSR can also be multi-frequency (as will be described later).

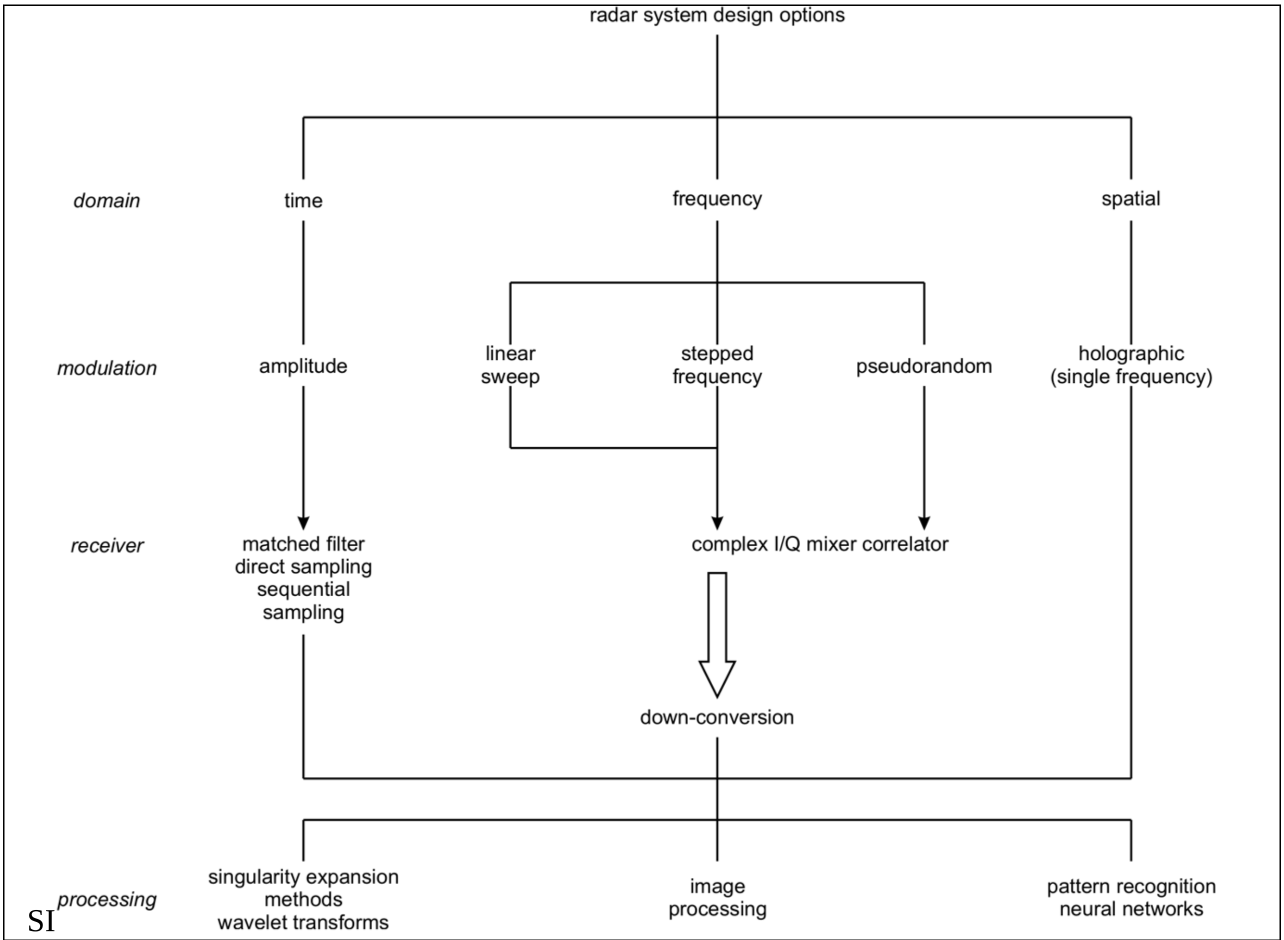

Fig. 1. Classification of main types of subsurface radar [2]

In optics, the term hologram means the recording of an interference pattern between two electromagnetic waves with one of them modulated by diffraction. The etymology of the term hologram comes from ancient Greek with the meaning "whole description" or "whole picture".

The first HSR may be the work of Keigo Iizuka who, with only the rudimentary technology available in the late 1960s, used polaroid film to register holograms from signals in the millimeter range at a frequency of 34 GHz [5], [6]. Due to the limitations of electronic technology at that time, the first subsurface radars were designed in CW mode, but it was immediately evident that for inspection of materials at great depth, attenuation of electromagnetic waves constituted a serious limitation to the development of applications for this tool. Also, due to the CW signal, it was not possible to compensate for attenuation with depth (or

Preprints (www.preprints.org) | NOT PEER-REVIEWED | Posted: 2 June 2021 doi:10.20944/preprints202106.0059.v1

distance) by applying a time-varying gain using front-end electronics [2], [7]. After later theoretical and experimental studies, a solution has been found for the realization of an HSR which that can be used to inspect media having low attenuation of electromagnetic waves at shallow depths. HSR of this type has many advantages because, by exploiting the phenomenon of interference, it can record the amplitude of the interference pattern for each position of a scanning antenna, and can therefore provide an image immediately at the end of the scanning of an area. The images thus obtained can be considered in real time as they do not in principle need any processing but only a device for recording the interference pattern (sensor + memory). It will be shown how this type of radar achieves a good compromise between maximum depth of investigation and high spatial resolution in the image plane [8].These qualities of HSR have, in particular, motivated research into their use for detection of land mines for military and humanitarian operations [9], [10], [11].

HSR differs from the two other types of GPR in that it provides plan-view (as opposed to cross-sectional) scanning of a surface to record subsurface radar holograms [8]. In this sense, HSR is analogous to the optical hologram technology firstly proposed and accomplished by D. Gabor in 1948 [12]. The method proposed by Gabor is illustrated by the example of recording a point target hologram as shown in Fig. 2.

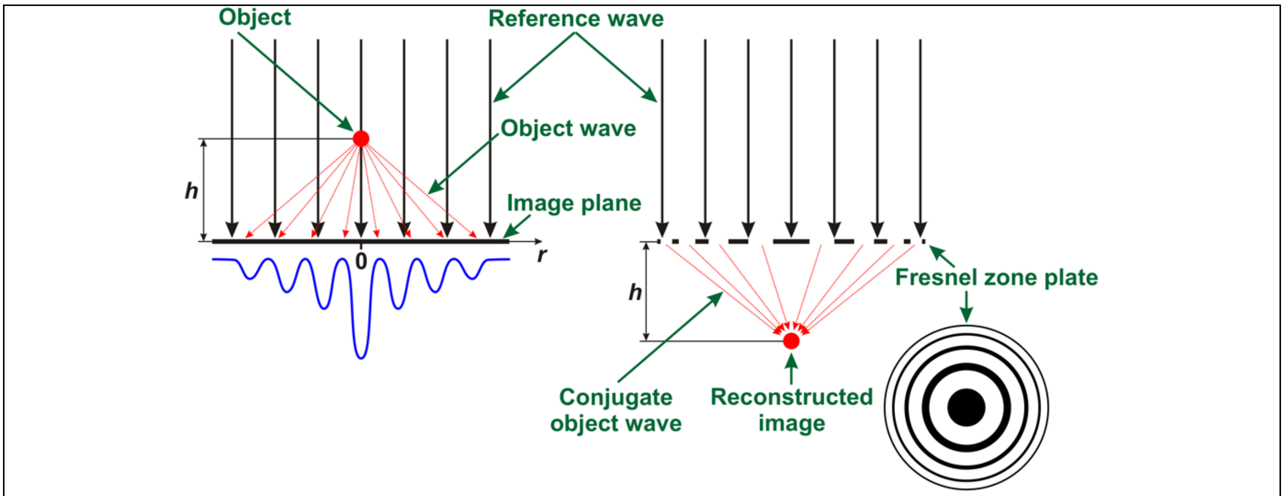

Fig. 2. Simplest optical hologram of a point object.

Considering a point reflector, a method of registering a hologram with properties of symmetry with respect to the target can be described. The interference between an incident reference plane wave perpendicular to the recording plane and the wave diffracted by the point reflector at a distance $\boldsymbol{h}$ from the plane, can be recorded as a variation in amplitude by an analog or digital sensor. It is assumed by convention that the reference plane wave has constant phase and amplitude $\boldsymbol{u_0}$.

We denote by $\boldsymbol{u(r)}$ the distribution of the amplitude of the diffracted wave which has the characteristics of a divergent hemispherical wave; this wave has an amplitude distribution defined by $\boldsymbol{u_1(r)}$ on the recording plane. The variation of this amplitude on the plane forms the holographic image.

$$u(r) = u_1(r)\exp(i\varphi(r)) \quad (1)$$

with phase $\boldsymbol{\varphi}$

$$\varphi(r) = \frac{2\pi}{\lambda}\sqrt{r^2 + h^2} \quad (2)$$

Preprints (www.preprints.org) | NOT PEER-REVIEWED | Posted: 2 June 2021 doi:10.20944/preprints202106.0059.v1

where λ is wavelength, and $\boldsymbol{r}$ is radius or distance on the recording plate from the axis of symmetry directly beneath the target. As a result of interference of these two waves ($\boldsymbol{u_o}$ and $\boldsymbol{u}$), the image plane records an intensity distribution I [13], [14].

$$I(r) = u_o^2 + u_1^2(r) + u_o u_1(r)[\exp(i\varphi(r)) + \exp(-i\varphi(r))]. \quad (3)$$

This equation describes a Fresnel zone plate [15] or interference pattern as shown in the right lower corner in Fig. 2.

To reconstruct a hologram, the recorded interference pattern is illuminated by wave $\boldsymbol{u_{or}}$ identical to the reference wave. So, directly behind the hologram, the distribution pattern looks like

$$u_p(r,0) = u_{or}[u_o^2 + u_1^2(r)] + u_{or}u_o u_1(r)\exp(i\varphi(r)) + u_{or}u_o u_1 \exp(-i\varphi(r)). \quad (4)$$

It is interesting to analyze the composition of the transmitted wave by evaluating the single terms of equation (4). The main component is the first term or the transmitted plane wave, also called reference. The second and third terms correspond instead to the virtual and real image of the object respectively.

The principle of the holography enunciated by Gabor in [13] had many disadvantages as a method for recording the hologram, with many limitations on the quality of images, and complexities that make practical application difficult. Thanks to the invention of the laser and its availability in laboratories, a solution was proposed by E.N. Leith and J. Upatnieks [16] who solved the limitations of the Gabor system. This method uses the properties of the coherence of the incident laser light source at a certain angle to the registration plate (or image plane), as shown in Fig. 3. Subsequent innovations in optical holography have similarly involved the use of different combinations of mirrors and beam splitters.

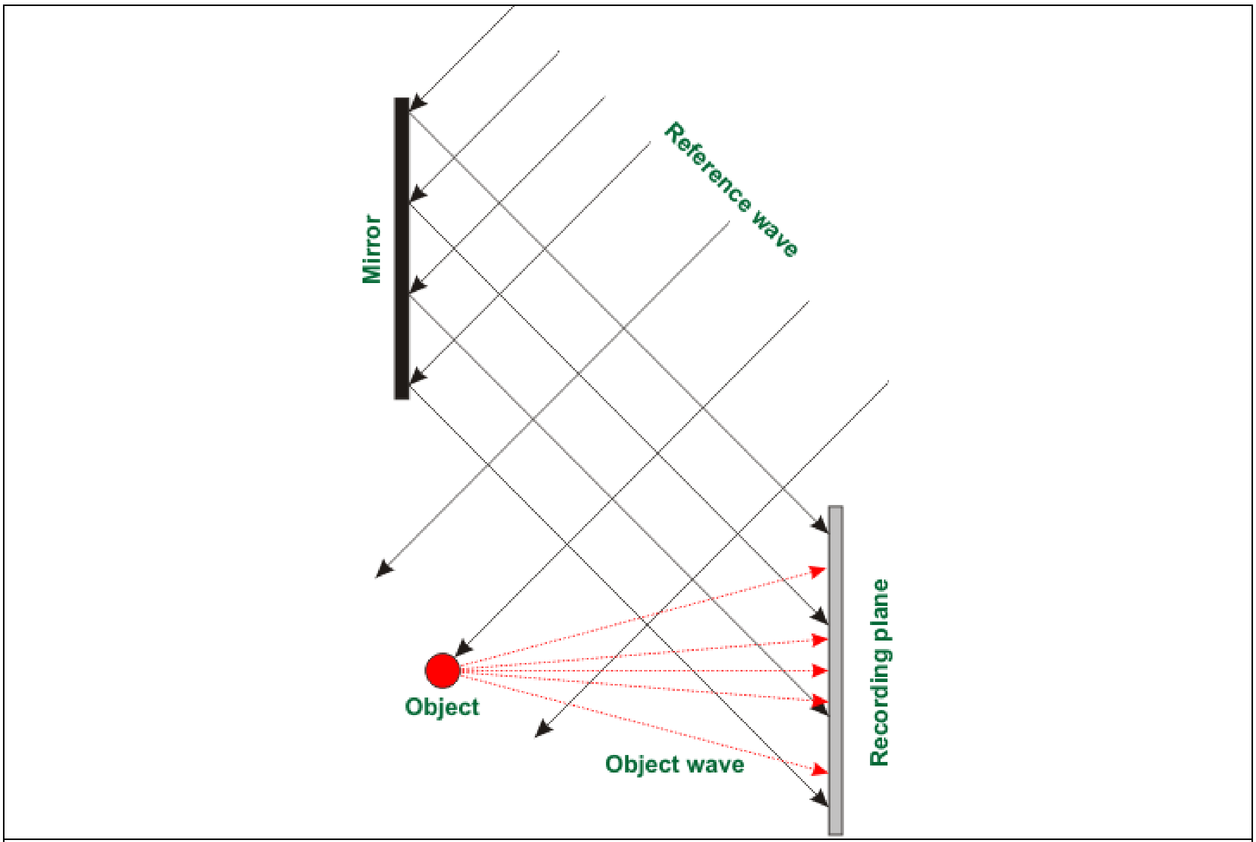

Fig. 3. Diagram of optical hologram recording with an inclined light beam (e.g. a laser source).

The experimental configuration that uses an inclined reference wave (see Fig. 3) is well suited to modern optical holography, since the attenuation of the medium (air) in the visible spectrum is negligible for the characteristic size of the system. In the field of aerial or satellite remote sensing, holographic radar has also been successful due to the very low levels of electromagnetic attenuation and dispersion in air and vacuum. For subsurface inspection of materials characterized by a much higher attenuation value ("lossy media"), at typical operating frequencies below 1 GHz, applications have been limited. One of the areas where the holographic method has found successful applications is security systems. In fact, holographic radar scanners have been designed that detect weapons hidden on passengers at airport boarding gates in close to real time [17], [18].

As described above, the systems for optical holography and microwave radar holography differ substantially in signal wavelength, and consequently the characteristic dimensions of the apparatuses for recording interference patterns. This difference can be estimated by the ratio between the characteristic dimension of the system d and the signal wavelength λ. For an optical system, $d/\lambda \cong 10^6$. This ratio for a holographic subsurface radar is less than 10 due to the high attenuation in lossy media requiring larger sources – almost comparable to the wavelength. Furthermore, the laws governing the propagation of electromagnetic waves also differ in the two cases: while the laws of geometric optics are valid for optical systems (see Figs. 2 and 3), these are not strictly valid for the analysis and development of HSR where attenuation, diffraction and near field coupling to the medium must be considered. Therefore, only the basic principles are common to optical holography and HSR. Nevertheless, the analogy is critical for understanding the physics of HSR, for interpretation of subsurface radar holograms, and for derivation of hologram reconstruction algorithms [8], [19], [20], [21], [22].

Although there are practical differences, it is interesting to compare optical holograms with radio holograms recorded by subsurface radar. The first optical holograms, which were recorded by D. Gabor and submitted in his classic work [12], are presented in Fig. 4.

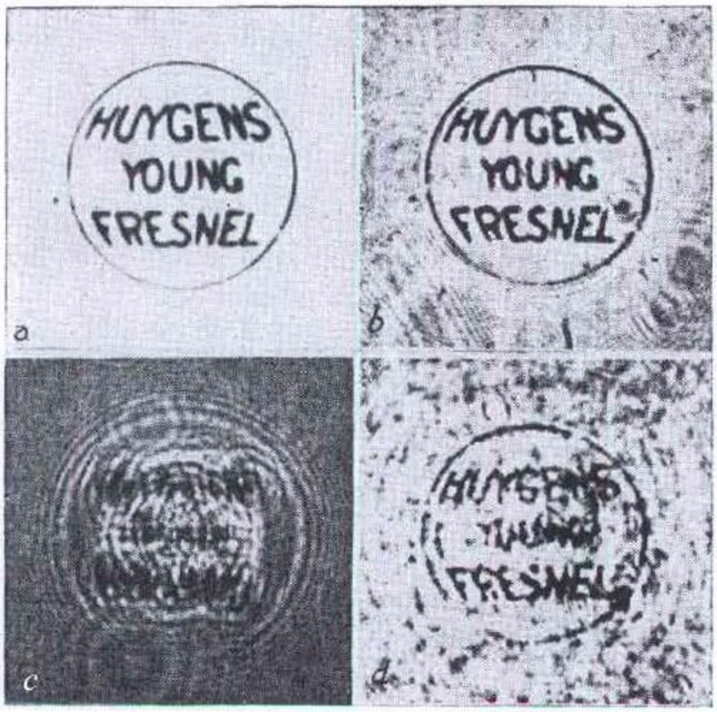

Fig. 4. Gabor's optical hologram [12]:

a) Original micrograph
b) Micrograph, directly photographed through the same optical system which is used for the reconstruction
c) Interference diagram
d) Reconstruction of the original; the letters have again become legible.

 doi:10.20944/preprints202106.0059.v1

To show an analogy to the optical hologram, an experiment was devised involving the recording of a hologram of a sheet of paper with metallic letters placed under the scanning surface. The shape of the letters was obtained by cutting a thin aluminum sheet to form the "RASCAN" with total width 44 cm and height 11.5 cm (see Fig. 5). The letters were glued on cardboard and covered with gypsum board sheets – each with a thickness of 12 mm. Scans were made for the different thicknesses (depths) obtained by adding one gypsum board at a time. On the surface, a manual scan was made over an area equal to 65 cm × 28 cm using RASCAN radar with CW operational frequency of 4 GHz.

To obtain an HSR image, it is necessary to perform accurate spatial sampling. Therefore, the holograms were recorded line-by-line at a fixed sampling step along parallel and equally spaced scanning lines; the radar head was moved manually along these parallel lines with sampling triggered by an optical survey wheel [23]. For avoiding distortions in the representation of the hologram image, the uncertainty of the spatial sampling must be much lower than the wavelength. The time to complete the scan depends on the size of the area and the number (spacing) of raster lines. Typically, for a 4 GHz RASCAN HSR, the distance between the parallel lines is 0.5 cm and this value is also used for the spatial sampling along the lines. Therefore, the image is composed of pixels having dimensions of 0.5 cm × 0.5 cm. The pixel size is chosen as a compromise between scan time and image quality. For this choice, we must consider the spatial resolution of the radar at the depths of investigation which depend on the type of antenna and on the frequency [24].

Fig. 5. Paper sheet with embedded aluminum foil letters that form the word RASCAN. Length of metal ruler is 12 inches or 30.48 cm.

In Fig. 6 we show selected images of eight microwave holograms at the 4 GHz frequency [8]. The first three images correspond to increasing thicknesses using 1, 2 and 3 gypsum plates. It can be seen that the word RASCAN is still legible. When the thickness of the gypsum plates increases (> = 4), there is blurring of the outlines of the letters, and the brightness (width) of the letters is no longer uniform. The explanation of these effects lies in the propagation of electromagnetic waves: At shallow depth, the reflection directed to the nadir from the metal surface of the letters has very high amplitude – and greater than the level of the reference signal and other reflections outside the nadir.

At greater depth (thickness), the radar antenna, due to its directivity, receives the reflections from the oblique edges (off-nadir) of the metal letters and the signal level begins to be comparable with the reference level – see equation (4). This phenomenon also explains the non-uniformity of the brightness (amplitude) of the letters which manifests as an undulation. At the maximum depth of about 10 cm obtained by stacking 10 gypsum plates, the image of the hologram obtained with the RASCAN radar resembles the optical hologram of Gabor. The comparison of the images shown in Fig. 4 and Fig 6 shows, albeit qualitatively, the differences between the holograms in the optical and microwave radar fields. Due to the different ratios between characteristic dimensions and wavelength for these holograms, the number of visible Fresnel zones varies greatly, from 3 to 4 orders or more for these two types of holograms.

HSR holograms	**Number of plaster sheets over letters**
	1
	2
	3
	4
	5
	6
	7
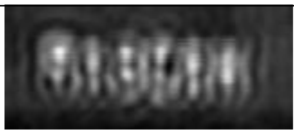	8

Fig. 6. RASCAN holograms recorded through varying stacks of plaster sheets.

When using HSRs for soil inspection, the medium may have low attenuation when dry and sandy, but may have high dispersion. In particular, the variability of the dielectric properties of these natural materials has a great influence on the quality of radar holograms. Experiments have shown that in many cases, this variability makes the interpretation of the hologram impossible. These studies, both theoretical and experimental, for the investigation of soils are available in various publications [7], [13], [19], [20], [25]. Since the attenuation of the medium and the heterogeneity of the surface characteristics are two factors that limit the maximum depth of penetration for an HSR, it must be remembered that the main advantage of an ISR is to be able to investigate great depths while maintaining a high contrast and signal-to-noise ratio thanks to the time-varying gain in a stroboscopic receiver, which amplifies more reflected signals that have a longer flight time. In a CW, system it is not possible to discriminate reflections by their time of flight, and therefore the use of HSR images is limited to reduced depths.

At the shallow depths where HSR is applicable, its main advantage is the ability to record images that have higher resolution in the plane of search (or plan-view) in comparison with ISR because of compact antenna appliance and easy choice of frequency range. High resolution in plan-view at shallow depths is extremely important for many applications, including:

- Diagnostics of composite materials in aerospace and other industries [26], [27], [28], [29], [30], [31], [32], [33], [34]
- Diagnostics of building details and constructions including cultural heritage monuments [35], [36], [37], [38], [39]
- Archaeological and paleontological imaging [40], [41], [42]
- Landmine detection and discrimination [9], [10], [11], [43], [44], [45], [46]
- Security systems [47], [48], [49], [50], [51], [52], [53]
- Detection of wood-boring insect damage [54]
- Medical imaging [55], [56], [57], [58], [59].

2. Holographic subsurface radar design

The main problem in designing a holographic subsurface radar is selection of the signal to use as the reference for recording the interference pattern. Usually, the generated signal is used. But the simplest way is to produce a coupling signal between the transmitter and receiver antennae. This requires an antenna appliance that can guarantee the independence of the phase and amplitude of this coupling signal from properties of the sounding surface and heterogeneities in the medium. To achieve this, for the RASCAN type radar, the antennae are mounted in a round, open-ended waveguide as in Fig. 7 [8], [60], [61].

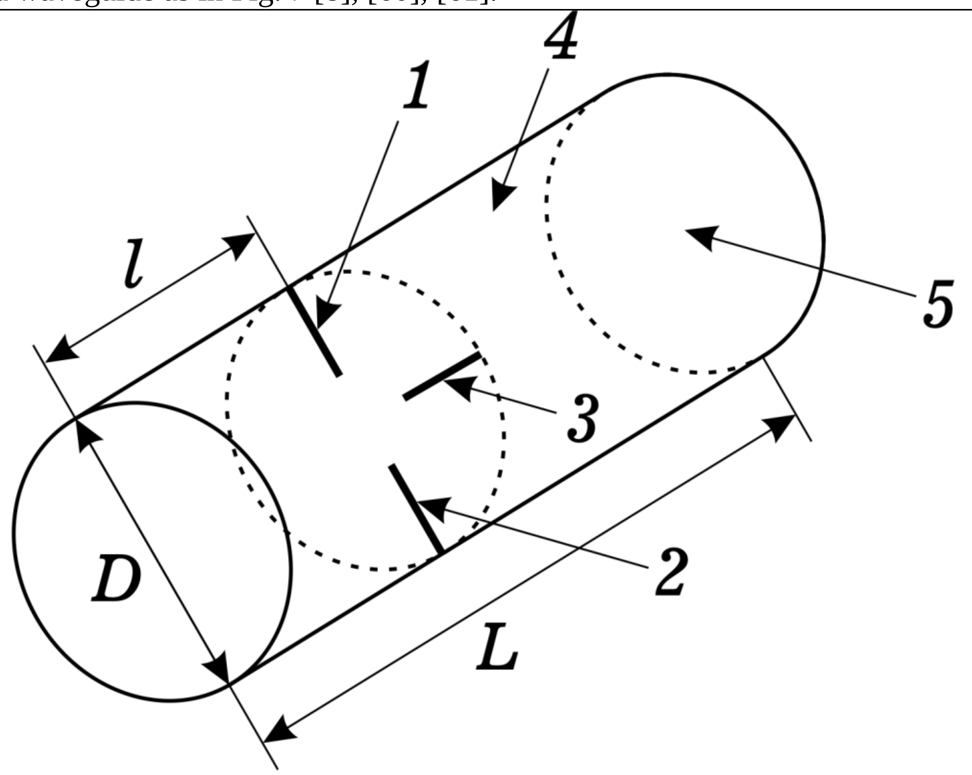

Fig. 7. Design of holographic subsurface radar antenna [60]:
1 – emitting feed antenna
2 – receiver feed antenna for parallel polarization

Preprints (www.preprints.org) | NOT PEER-REVIEWED | Posted: 2 June 2021 doi:10.20944/preprints202106.0059.v1

3 – receiver feed antenna for cross polarization
4 – round waveguide
5 – open end of waveguide
D – waveguide diameter
L – waveguide length
l – distance between closed end of waveguide and plane of pin antennas 1 and 2.

Initially, two receivers were used: for parallel and crossed polarizations. In this case, images were recorded simultaneously for both polarizations and for several frequencies [39]. The recording of cross polarization enhanced detection of elongate targets by reducing the influence of the angle between the long axis of the object and the plane of the receiving antenna feed.

This scheme is quite simple, but it allows recording of only amplitude radar holograms. This is sufficient when registering holograms in media with a high dielectric constant ε and a high level of attenuation of electromagnetic waves [19], [20]. In this case, there is no wave structure or outer Fresnel zones in the recorded image (see Fig. 8), and digital reconstruction of the radar hologram does not significantly improve the image. The interference pattern alone provides a good approximation of the target shape in plain view.

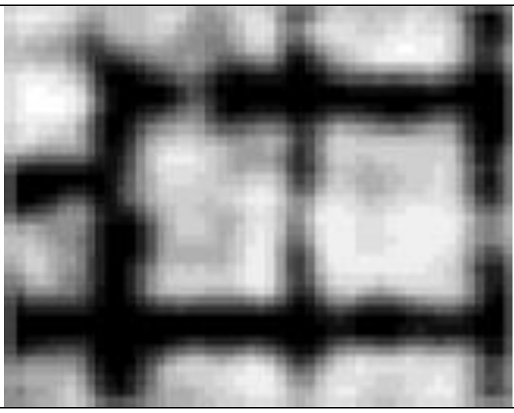

Fig. 8. Radar image recorded at 3.9 GHz frequency on reinforced concrete wall. The reinforcing mesh spacing in the wall was 0.2 m by 0.2 m and the thickness of the protective concrete coating over reinforcement varied from 3 cm to 4 cm [39].

Another feature of images recorded at crossed polarizations is the absence of symmetry for point targets as in Fig. 9b. In this case, the interference pattern depends on the orientation of the antenna when scanning the surface of the examined medium. At the same time, at parallel polarization (Fig. 9a), the symmetrical concentric circles in the interference pattern are directly analogous to the optical image in Fig. 2.

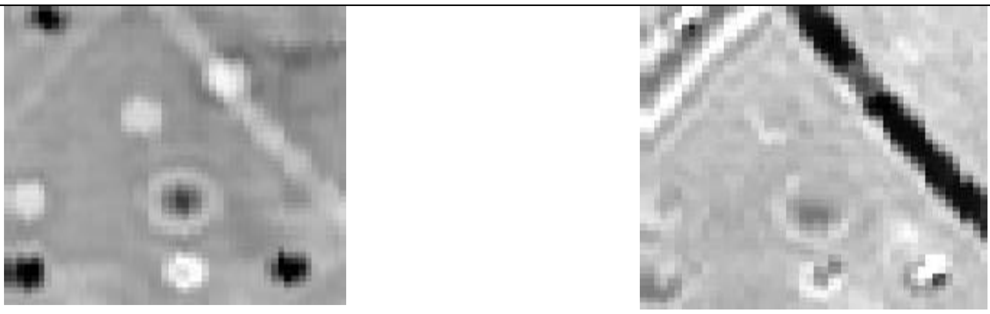

a) b)

Fig. 9. Parallel a) and cross b) polarization of received signals recorded by RASCAN at frequency of 4.0 GHz [39]. These images were recorded for a test wall inside of which small

Preprints (www.preprints.org) | NOT PEER-REVIEWED | Posted: 2 June 2021 doi:10.20944/preprints202106.0059.v1

coins and metal wires were placed at different depths.

The RASCAN radar has been designed with programmable electronics capable of emitting a series of discrete frequencies in sequence (up to a maximum of 5). This operating mode, also called multifrequency, is fundamental for an HSR that is based on a principle of monochromatic (or CW) function, as the response in reflection from objects at certain depths can be zero due to the sinusoidal dependence of sensitivity on the distance (depth) of the object: for a frequency value and a medium with a constant propagation speed, there will be repetitious distances (depths) that provide a phase which cancels the sinusoidal function and therefore the detection of the object [62]. The effect of changes in contrast with frequency is demonstrated in an animation [63]. This animation recorded by RASCAN HSR presents a multi-frequency hologram of a rectangular Soviet PTM-3 antitank mine buried in sand. Each frame of the animation corresponds to a selected frequency of the radar. It can be seen that there are frequencies at which the mine is clearly visible, and others where it nearly disappears.

Therefore, by selecting the discrete frequencies within the antenna band [64] and comparing the images obtained at the different frequencies, it can be assumed that the reflection from an object at a given distance from the antenna will always be visible for at least at one frequency.

For the simplest case of a single frequency (CW) HSR, a mathematical model is reported below. Consider a reflector (target) plane perpendicular to the propagation direction of the incident electromagnetic wave generated by the holographic antenna. The waves emitted by the HSR have a constant frequency ω, amplitude and phase that are not constant over time. $\boldsymbol{A_r}$,is defined as the amplitude of the reflected wave of constant value, and with phase φ_r depending on the depth of the plane reflector.

$$\varphi_r = 2\sqrt{\varepsilon}\frac{l\omega}{c} + \Delta\varphi \,, \qquad (5)$$

where $\boldsymbol{\Delta\varphi}$ is the phase shift which arises upon reflection of the electromagnetic wave from the object, $\boldsymbol{\varepsilon}$ is the dielectric permittivity of the medium, $\boldsymbol{l}$ is the distance to the object, ω is the angular frequency, and $\boldsymbol{c}$ is the speed of light. Thus, the reflected signal as a function of time $\boldsymbol{t}$ can be written as

$$A_r\cos(\omega t + \varphi_r) \qquad (6)$$

Reflected wave (6) mixes with a constant-phase radar reference signal of the form

$$A_o\cos(\omega t + \varphi_o), \qquad (7)$$

where $\boldsymbol{A_o}$ and $\boldsymbol{\varphi_o}$ are the amplitude and phase of the reference signal, respectively. The reflected signal (6) is mixed with the radar reference signal (7) at the receiver. The amplitude of the signal in the mixer output at the difference frequency is given by

$$A_rA_o\cos(\varphi_o - \varphi_r). \qquad (8)$$

From this relation one can conclude that, if the phase shift between the reference signal and reflected one is close to

$$\varphi_o - \varphi_r = (k + 1/2)\pi \,,\ k = 0,1,2,\ldots \qquad (9)$$

the level of recorded signal from the object is low, and at

$$\varphi_o - \varphi_r = k\pi \,,\ k = 0,1,2,\ldots \qquad (10)$$

the recorded signal level is maximal. These circumstances have been observed experimentally [39]. To avoid “blind” depths the original RASCAN type HSRs used multiple discrete frequencies across a bandwidth that ensured high target contrast for one or more images [64].

3. Reconstruction of subsurface radar holograms

Preprints (www.preprints.org) | NOT PEER-REVIEWED | Posted: 2 June 2021 doi:10.20944/preprints202106.0059.v1

Typical surveyed media (soils, concrete, etc.), often have a relatively high dielectric constant due to moisture content, which also enhances electrical conductivity, and therefore attenuation. As described previously, this makes it difficult to register the outer Fresnel zones or wave picture, and sometimes makes it impossible, with the subsurface object observed only on the axis of the antenna pattern [19], [20].

However, for media with a high degree of transparency for microwaves and a low level of ε, reconstruction of the hologram from a relatively complete interference pattern significantly improves the quality and resolution of HSR images [21]. To achieve this, a modification of the RASCAN-5 HSR with corresponding software was developed (Fig. 10). The general layout of the radar antenna was retained, but the crossed polarized antenna channel was eliminated, and the generator signal was used as a reference signal. This allows recording of complex microwave holograms of hidden objects. The radar antenna head containing both transmitter and receiver is connected via cable to a microcontroller unit with a USB link to an ordinary computer. The microcontroller unit drives the transmitter and receiver, digitizes data, and transmits them to the computer.

Fig. 10. Holographic Subsurface Radar (HSR) RASCAN-5 as it is supplied to customers [65].

The RASCAN-5 model allows the acquisition of complex holograms generated by the microwave holographic interference of shallow-depth objects with different shapes. In the event that the attenuation of the medium and the characteristics of the antenna reduce (or ideally cancel) the external fringes of the interference pattern [8], and then the holographic image will be a good reproduction of the shape of the object itself. Furthermore, in the case of microwave transparent propagation media, hologram reconstruction algorithms can be adopted [21], [50], [66], [67], [69]. With these elaborations, it is possible to improve the resolution of the microwave images at different depths of investigation. For example, Fig. 11 illustrates the data acquisition method for reconstructing the microwave hologram of an object that has a two-dimensional shape at a depth z_0.

Preprints (www.preprints.org) | NOT PEER-REVIEWED | Posted: 2 June 2021 doi:10.20944/preprints202106.0059.v1

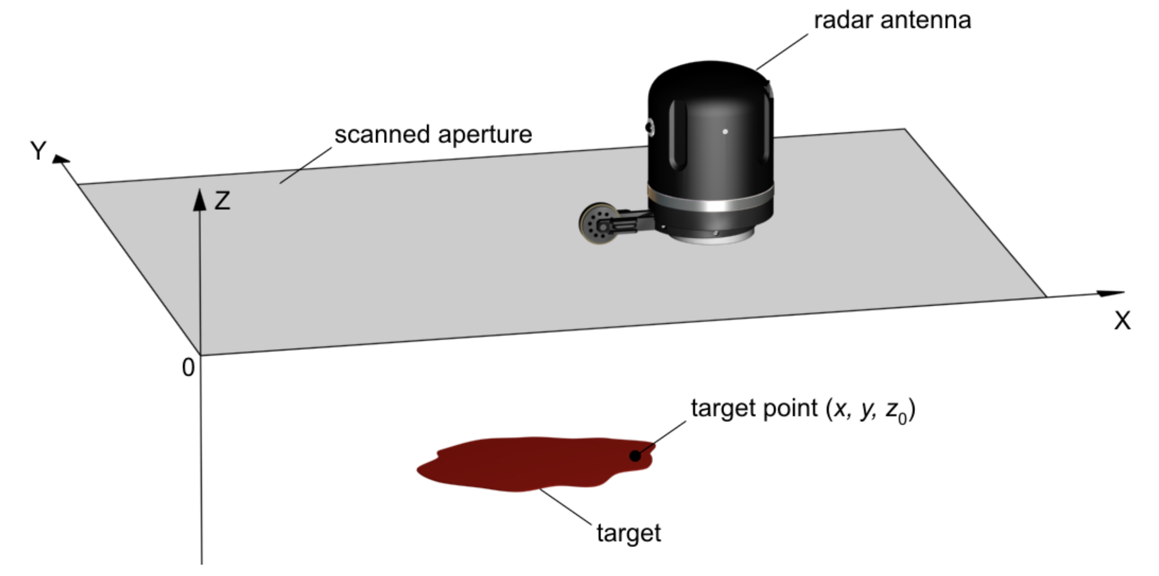

Fig. 11. Geometry of holographic imaging system.

The target is assumed to be flat, parallel to the scanning plane, lying at a constant depth z_0. The key relationships can be summarized as follows:

$$F(k_x,k_y)=\frac{1}{(2\pi)^2}\iint E(x,y)\,e^{-i(k_x x+k_y y)}dxdy \qquad (11)$$

$$S(k_x,k_y,z_0)=F(k_x,k_y)\,e^{i\sqrt{4(\omega\sqrt{\varepsilon}/c)^2-k_x^2-k_y^2}\cdot z_0} \qquad (12)$$

$$E_R(x,y,z_0)=\iint S(k_x,k_y,z)\,e^{i(k_x x+k_y y)}dk_x dk_y \qquad (13)$$

where E (x, y) is the recorded hologram.

E (x, y) represents a complex quantity whose values are sampled by the holographic antenna on the opening of the scanning area whose plane has coordinate z = 0; applying the Fourier transform to E (x, y) in the space domain (x, y) we obtain the distribution F (k_x, k_y), that is the spectrum of the plane waves of the hologram; k_x and k_y represent the wave numbers corresponding to x and y respectively. At a different coordinate z_0 of a parallel plane it is possible to calculate the spectrum of the plane waves of the hologram S (k_x, k_y, z_0). From the latter, by means of the inverse Fourier transform, we can obtain ER (x, y, z_0), which represents the holographic image for $z = z_0$. The mathematical formulation of the calculation process is described by equations (11), (12), (13).

Remembering that HSR operates in CW mode, to obtain the image of the object, its depth must be known a-priori, as well as the speed of propagation in the medium. In the case that these parameters are not known, or a rough estimate is known, this calculation method can still be adopted by repeating at various depths and verifying the value for which the image represents the reconstructed hologram with the best focus. In more complex experimental situations such as non-homogeneous dielectric media and with high attenuation levels, the method iterated over more depths provides the result with the best focus on the artifact. In general, the determination of the depth of a buried object through measurements with ISR or HSR is typically a difficult problem since the measurements in reflection are performed on a half-space and this requires the solution of an inverse and ill-posed problem [70]. Another reconstruction algorithm based on Green's formula was proposed in [71]. Kirchhoff approximation [72] and less strict empirical algorithms used for the reconstruction of microwave holograms of landmines was described in [44] and [73].

Often, the scanning is performed on an uneven surface, which adds additional difficulties in obtaining accurate radar images of subsurface objects. This is especially true when detecting plastic cased landmines that have a minimal signature in MW range and are located close to the scanned surface. The problem of reconstructing MW holograms for media with an uneven surface was considered in [74], [75] and [76].

4. Main applications of holographic subsurface radars

The dominance of impulse subsurface radars in the GPR market [77], [78] is explained, as mentioned earlier, by their ability to provide a greater effective depth of sounding. HSRs, by virtue of their specificity, are preferred in an application niche where it is sufficient to inspect the shallow subsurface, but high resolution is needed.

In early development and testing of HSRs, the detection of landmines [45], [79], and plastic and metal pipes in a concrete floor screed [7], [31] were promising applications. Further research has expanded the scope of HSRs, many of which are also described in [80]. Below, we will consider the main applications of HSR, for which significant experimental results have been demonstrated.

4.1. Landmine detection

In the latter two thirds of the 20th Century conflicts all over the world were characterized by widespread use of both antipersonnel and antitank mines. From the 1960s on, a significant proportion of deployed mines had plastic casings, and some had almost no metal, making them difficult to detect. Although use has declines since the 1998 Ottawa mine ban treaty an estimated tens of millions remain in over 60 countries worldwide. Most victims of mines are civilians since military personnel are trained to avoid them, and have teams dedicated to their detection and demolition. Since mines can remain dangerous long after a conflict has ended, civilians, many of them women and children, are the main casualties of mines. But it is not just mines; there are many explosive remnants of war. For example, in Europe there is unexploded ordnance (UXO) still undetected and dated as far back as World War I. According to the Landmine Monitor, global mine casualties reached a minimum in 2013, and have risen steadily since [81]. Armed conflicts are wide spreading in the world including Afghanistan, Iraq, Mali, Libya, Myanmar, Nigeria, Syria, Ukraine and Nagorno-Karabakh.

Significant material damage is inflicted as vast plots of land are removed from safe agricultural use until they are completely demined. For this reason, the rural populations in some parts of Africa and Southeast Asia are saved from starvation only through international aid.

The use of antipersonnel mines in armed conflicts unfortunately is still driven by reasons including the simplicity of design and that deployment can be accomplished by minimally trained personnel. In addition, low production costs allow the purchase of large lots at an affordable price even for terrorist organizations. UN estimations give the cost of some types of antipersonnel mines at around $3, while the cost of anti-tank mines rises to about $75. On the other hand, the cost for removal is certainly much higher and can be estimated at around $300. On average, according to UN estimates, the average costs for demining are about $ 0.6 per 1 sq m, with a daily coverage for a single operator of between 10 sq m and 20 sq m [82]. Human losses during demining are unfortunately still high and vary from country to country, but approach 1 to 2 deaths for every 1,000 mines removed.

The widespread introduction of plastic bodied mines into the arsenals of the world's armies made it necessary to develop means for their detection. Traditional metal detectors have proven to be practically ineffective due to the low metal content of some mines. It should be noted that the German army already during World War II used mines in with wooden casings (the infamous Schu-42 mine), which injured many sappers who were armed only with metal detectors. To detect mines with a low metal content, different armies of the world began in the 1980s to use radio wave mine detectors, which worked on the principle of detecting variations in the dielectric constant ε of the soil caused by the presence of a mine [45].

Preprints (www.preprints.org) | NOT PEER-REVIEWED | Posted: 2 June 2021 doi:10.20944/preprints202106.0059.v1

The main problem with using radio-frequency devices for detecting plastic mines with a low signature is a high level of false alarms caused by both natural ground inhomogeneities and an uneven of the ground surface. Experience shows that with a false alarm level of 1 to 2 per 1 square meter, a sapper will reject the high-tech device and prefers to work with a simple probing spike – which is dangerous because it puts the sapper very close to potential mine and may trigger its detonation by spike. One of the ways to reduce the level of false alarms is to obtain an image of a target while it is still in the ground, which allows reduction of false signals from ground inhomogeneities [46], [79], [83].

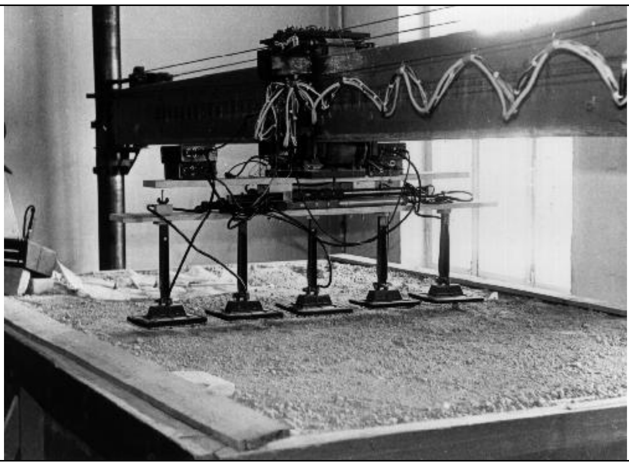

Fig. 12. Mock-up of the wide-span system for mine detection.

Fig. 12 depicts a laboratory set-up of a wide-span mine detection system that was designed in the late 1980s [45], [46]. In this set-up, several standard mine detectors with operating frequency of 600 MHz were used. The advantages of wide-span systems include their higher efficiency and the possibility to reduce the probability of false alarms during the mine clearance due to accurate spatial data. Mines can be distinguished from the local heterogeneities of the soil by their shape and size because the characteristic size of an antitank (20 cm to 30 cm diameter) and antipersonnel (7 cm to 12 cm) mines is known [84].

The area covered by the scan with the wide-span mine detector mockup (see Fig. 12) is 2 m × 6 m and the depth of the tank with soil 1.5 m. Fig. 13 shows one of the first results from radar array scanning of two mines in the center of the image; one metal anti-personnel TM-62M (left side) and the other a TC-6 plastic anti-tank mine (right side). In addition to these two targets there are "clutter" objects such as a piece of metal pipe in the lower left corner of the image, a 30 x 30 cm^2 metal plate in the lower right corner and a brick is upper right corner. The depths of these objects vary from 5 to 10 cm.

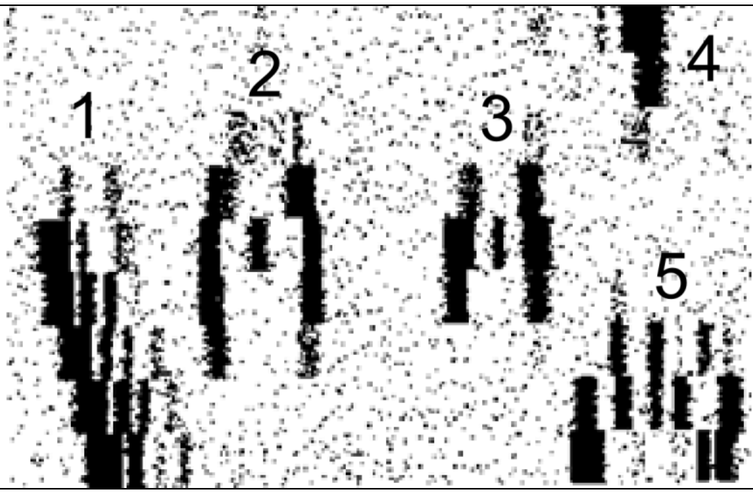

Fig. 13. Radar images recorded by wide-span mine detector:

1 – metal pipe
2 – metal-case antitank mine TM-62M
3 – plastic-case antitank mine TC-6
4 – brick
5 – metal plate.

The radar images in Fig. 13 show in black-and-white the amplitude of the signals reflected and recorded with the microwave antenna array. The image of a mine has two opposing arcs perpendicular to the direction of the array movement, and in the center an intense reflection. This characteristic response allows classification of the object as a mine with a cylindrical container and in the center the pressure plate for detonation, the estimated diameter from 20 cm to 30 cm is consistent with the anti-tank mine. The use of such a scanning system has shown with further experiments that it tolerates well the effects of inhomogeneity of the soil for mine detection (Target 1 and 2) and classification against clutter targets (Target 3, 4, 5)

A spatial filtering algorithm has been developed and tested that “identifies” buried mines by the characteristic shape of their response to microwave radar scanning. For this purpose a simple correlation filter has been designed with a recognition matrix $\mathbf{F}_{j,n}$, which depends on the shape and dimensions of the selected targets [45], [46].

$$\mathbf{F}_{j,n} = \left\| f_{j,n} \right\| = \left\| \begin{matrix} 0 & 1 & 1 & 1 & 0 & 0 & 0 & 0 & 1 & 1 & 1 & 0 \\ 1 & 1 & 1 & 0 & 0 & 1 & 1 & 0 & 0 & 1 & 1 & 1 \\ 0 & 1 & 1 & 1 & 0 & 0 & 0 & 0 & 1 & 1 & 1 & 0 \end{matrix} \right\|; \quad \begin{matrix} j = 1,2,3; \\ n = 1,2,...12. \end{matrix} \tag{14}$$

The following algorithm was then provided for target recognition. This describes the relation between each element of the radar image brightness matrix $\left\| m_{i,k} \right\|$ and the element of the matrix $\left\| f_{i,k} \right\|$, which is calculated as follows:

$$l_{i,k} = \Theta\left(\sum_{j=1}^{3} \sum_{n=1}^{12} f_{j,n} \cdot m_{i+j-2,k+n-5} - p \right), \tag{15}$$

where: $\boldsymbol{p}$ is the value of the detection threshold.

The function Θ(x) in equation (15) is determined as follows:

$$\Theta(x) = \begin{cases} 1; & at\ x > 0. \\ 0; & at\ x \le 0. \end{cases}, \tag{16}$$

Also, it should be noted that the calculated values of the matrix M=$\left\| m_{i,k} \right\|$ may go beyond the region where it is defined. In this case, the corresponding values of the matrix are taken to be zero. The proposed algorithm made it possible to recognize both anti-tank and anti-personnel mines in this experimental setup. Considering the relative crudeness of computers and displays, and the general novelty of using computers to evaluate image data in the late 1980s, these results were very encouraging at the time.

Further advances were made with the development of HSRs of the RASCAN type in the mid-1990s [79]. The design of RASCAN radars was quite simple and could be easily adapted to any desired frequency range.

The prototype of a wide-span mine detector MiRascan included elements for detecting five frequencies of HSR in two orthogonal polarizations, and a metal detector [79]. The sensors were installed on a cart, which was driven by a stand-off operator using control box connected by an umbilical cord (Fig. 14a). A block diagram of the MiRascan radar with metal detector is presented in Fig. 14b.

Preprints (www.preprints.org) | NOT PEER-REVIEWED | Posted: 2 June 2021 doi:10.20944/preprints202106.0059.v1

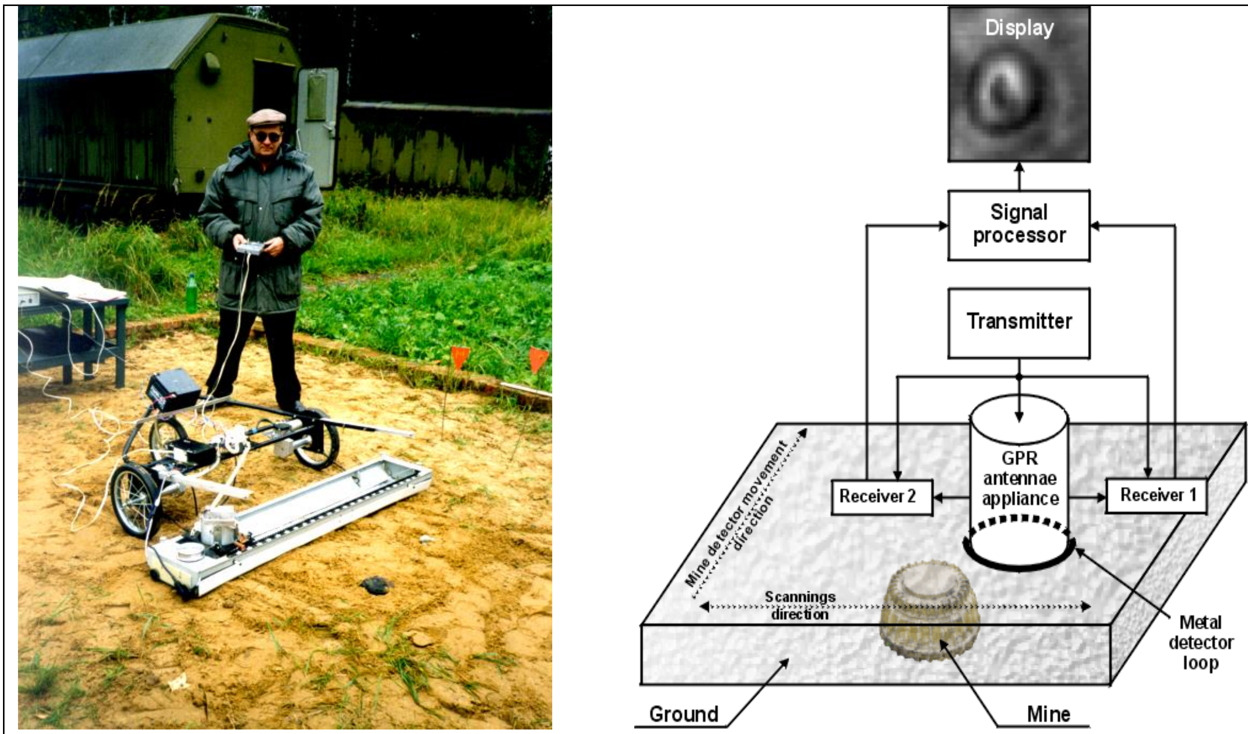

a) b)

Fig. 14. a) Two-sensor MiRascan mine detection system; b) block diagram of MiRascan radar with metal detector.

The radar operated at five frequencies in the range of 1.6 through 2.0 GHz and transmitted unmodulated signals at each frequency. Its signals were received in two polarizations. Power emitted by the generator for each frequency was cycled in sequence, and produced only 10 mW, providing complete safety for the operator. An induction loop metal detector was located on the aperture end of the radar, providing spatial coincidence of the HSR and metal detector images. The operating frequency of the induction metal detector was 2 MHz, and the diameter of the induction loop was the same as radar antenna at 120 mm. The cyclical recording of signals at each frequency and both polarizations of HSR and from the metal detector was realized at a high rate ensuring accurate registration of all images. Scanning in the cross-track direction was accomplished by electromechanical movement of the HSR/metal detector head, while along track movement was simply due to the advancement of the entire device at speed of 1 m per 6 minutes. The prototype mine detector could survey a lane with a width of 112 cm.

Inert (training) Soviet TM-62M and PTM-3 and the Italian-made TC-6.1 were used in testing as metallic-body antitank mines. Italian TC-2.5 and Soviet TM-62PZ antitank mines simulated plastic-body mines. As examples of antipersonnel mines, Soviet plastic-body PMN-2 type mines were used. A plastic-body MS-3 booby trap was also used. All these mines are shown in Fig. 15.

Fig. 15. Mines used in experiments.
1 – TC-6.1, 2 – TC-2.5
3 – TM-62M, 4 – TM-62PZ
5 – PTM-3,
6 – MS-3, 7 – PMN-2 (two mines).

The experiments to detect and identify inert plastic- and metal-cased mines were conducted under realistic conditions in a special military test ground near Moscow. The proving ground had sites with several characteristic soils: sand, chernozem, loam, etc. This ensured testing across wide variations in soil dielectric properties. In order to research the impact of moisture content on the quality of images received by the different channels, tests were conducted under differing weather conditions: both during hot/dry periods, and following rain events.

Since many mine fields have been placed in populated areas, objects of anthropogenic origin or clutter produce false alarms that often outnumber actual explosive threats. To test discrimination between mines and clutter, glass and plastic bottles (empty and filled with water) were buried in the test bed. The antitank mines and the bottles were laid in the ground at a depth of 5 cm to 10 cm, and for the antipersonnel mines a depth of 1 cm to 5 cm.

The experimental results are shown in Fig. 16 for two polarizations of HSR (the left images are for the cross-polarization of received and transmitted signals and the center images are for parallel polarization). The right column images were recorded by the metal detector. Although HSR images were recorded at five discrete frequencies, only the most distinct image is shown for each polarization. The plastic MS-3 booby trap images are presented in upper row of this figure. High contrast in the metal detector (top right) is explained by the presence of a metal ring around the casing.

Radar image (cross-polarization)	**Radar image (parallel-polarization)**	**Metal detector image**

Images of MS-3 booby trap in chernozem

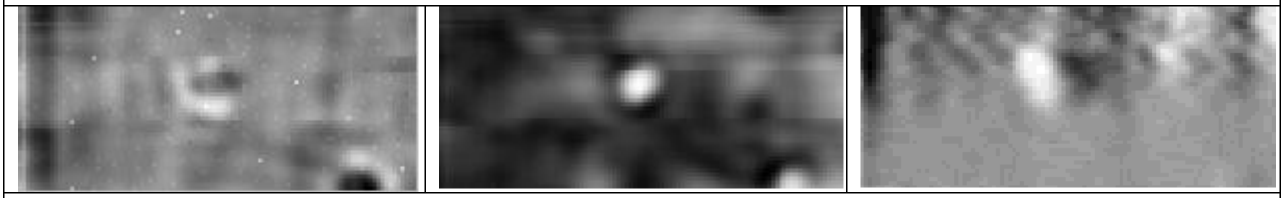

Images of two PMN-2 antipersonnel mines in chernozem

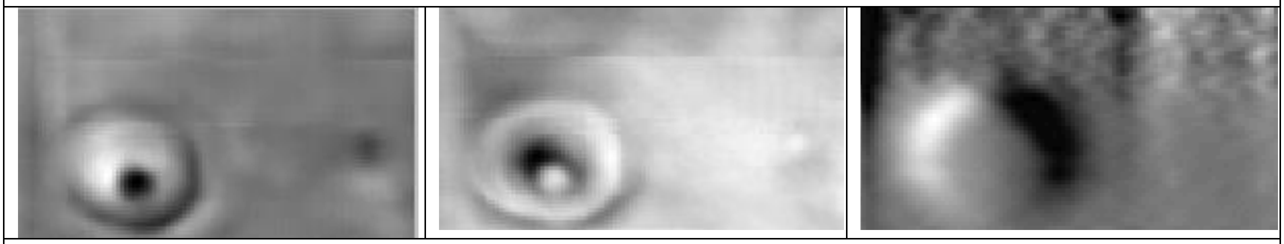

Images of Russian antitank mine type TM-62M

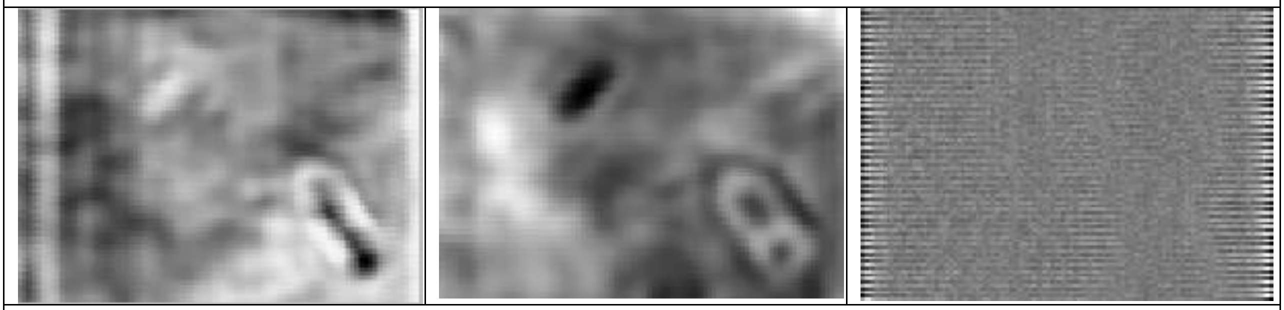

Images of glass and plastic bottles filled with water in sand

Fig. 16. Objects images detected by HSR and metal detector

In the second row of Fig. 16, two PMN-2 antipersonnel mines are shown, one of which was fully armed (at the top of the image), and the other (on the bottom) with the metal detonator removed. In the HSR images, both mines are seen (albeit in lower contrast for the minimal metal mine), while the metal detector depicts only the complete mine.

The results of scanning a Russian TM-62M antitank mine are shown in the third row of Fig. 16. For this metal-cased mine, the round form is clearly seen in all channels, with the raised pressure plate clearly visible in the HSR images. The bottom row presents the images of glass (top of each image) and plastic (bottom of each image) bottles filled with water. Since the bottles have no metal, there is no apparent target on the metal detector image. It is worth noting that in the years after this test, approaches which merge or fuse two sensors outputs were adopted for other dual-sensor mine detectors such as Minehound [85], and ALIS [83].

Further experiments with higher frequency RASCAN radar provided further MW holograms of explosive devices as shown in Fig. 17 [86]. The items were buried horizontally in a sand test bed, and scanned with a RASCAN-4/4000 at frequency of 3.8 GHz. In general, large explosive objects are buried at varying depths, as in the case, for example, the ends of the object ranged

 doi:10.20944/preprints202106.0059.v1

from zero to about 8 cm. In particular, the rocket's fins were almost exposed, while the cylindrical body was about 7 cm deep. The thickest part of the 8-cm shell body was on the surface, with the fins at about 4 cm and the thinnest part of the body at 7 cm or 8 cm. This information is used to understand how the various parts of the body reflect / diffuse plane waves and the figures shown show the wave nature of the interference pattern acute with a RASCAN type HSR. However, considering the response of the first lobe of the interference pattern, the 2D images faithfully reproduce the shape and size of the real target, even though the 3D reconstruction of the hologram from the recorded interference pattern has not been performed.

Photo	**Radar hologram**
	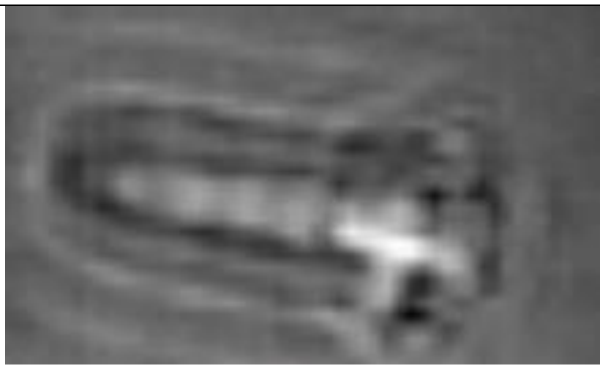
50 mm rocket	
	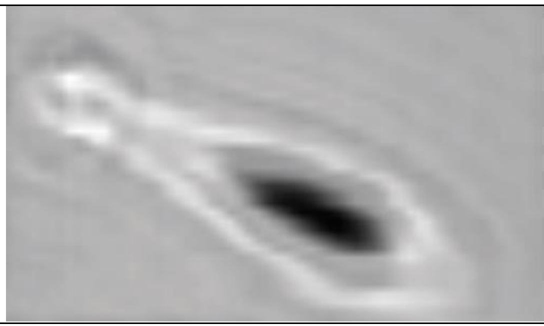
80 mm shell	
Fig. 17. Microwave hologram images recorded by RASCAN-4/4000 subsurface radar	

It has been shown that HSR images of mines are sufficiently distinct from common clutter items, that they can be discriminated using a machine learning neural network approach. In a study using a cylindrical mine simulant and four clutter objects (rock, crushed can, shell casing and segment of barbed wired), a neural network was trained to identify in any HSR image the mine with 100% detection rate, and zero false alarms [87].

HSRs of other designs intended for mines detection were described in [10], [11], [44]. The operational frequency for these radars is 2 GHz. In most conditions, this seems to be the optimal frequency for land mine detection [79], [88]. The HSR for mine detection developed in China [10] is shown in Fig. 18. For signal registration, the spiral scanning method was used, with the device attached to a rail rotating around the mounting axis as shown in Fig. 18 (right). In this case, the MW hologram is recorded in polar coordinates.

The advantage of this scanning method is its relative simplicity and higher productivity in comparison with a rectangular grid, while the disadvantage is the presence of a blind zone in the center of the scan, as well as the necessity to place the central pivot within a potentially mined area. So, it is difficult to imagine how to use such this technology in actual field conditions.

Fig. 18. HSR designed for mine detection [10].

Rail system for spiral scanning

The simple and compact design of the RASCAN HSR suggested another approach for alleviating the burden of manual scanning using a robotic scanner (as shown in Fig. 19 below) with simple architecture for sweeping the radar antenna across the path of the robot as it advances incrementally [89].

Fig. 19. HSR on a robotic scanning platform [89].

Another project also uses holographic subsurface radar as one of the sensors. This is a complex device that consists of HSR with an operating frequency of 1.97 GHz, impulse GPR with a sophisticated antenna system, which includes one transmitting and four receiving antennas, and a video camera, Fig. 20 [88], [90]. The impulse radar antenna system allows measurement of the 3-D Cartesian coordinates of detected objects. The HSR scans the area and subsequently produces plan-view images of the subsurface object detected by the impulse GPR. The idea to use both types of radar was proposed for reducing false alarms from systems based on impulse GPR alone. All sensors were mounted on a commercial robotic platform (model Jackal, from Clearpath Canada). The antenna of the HSR was similar to the antenna proposed in [60], used in [79] and depicted in Fig. 7. Note that all of the HSRs described above used practically the same frequency range of 2 GHz. This is due to the need to provide sufficient resolution to detect and discriminate land mines, while at the same time maintaining sufficient sounding depth of 5 cm to 20 cm.

Preprints (www.preprints.org) | NOT PEER-REVIEWED | Posted: 2 June 2021 doi:10.20944/preprints202106.0059.v1

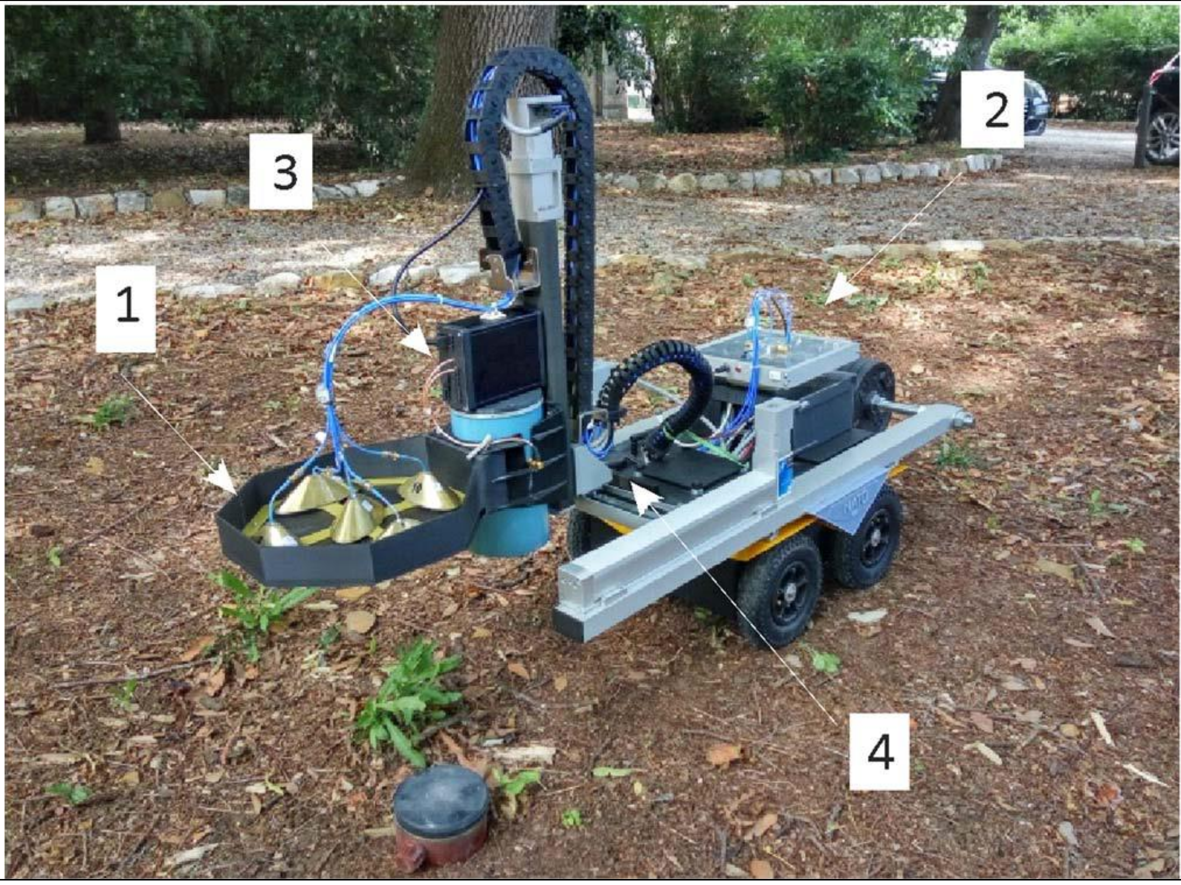

Fig. 20. Robotic platform "Ugo 1st" [90]:
1 – Impulse GPR antenna system
2 – Impulse GPR hardware unit
3 – Holographic radar
4 – 3-D camera/scanner.

The task of humanitarian clearing of vast territories is urgent. Intensive attempts to apply subsurface radar technology for combat and humanitarian demining have been undertaken since the 1980s. However, the results so far are limited, and not yet widely used in either military or humanitarian efforts. The military of many countries have sufficient means and special training to perform demining in the course of hostilities. However, humanitarian demining, after hostilities have ended, has special requirements that restrict possible methods. For example, it is impossible to use explosives or mechanical flails or plows to make safe lanes through minefields. All mines must be cleared, and explosive or mechanical methods are not suited for urbanized areas.

The situation is complicated by the fact that the greatest danger to civilians is posed by plastic anti-personnel mines, which, due to their insignificant signature on both metal detectors and many radars, are easily confused with reflections from soil irregularities. A logical solution to the problem would be a strict ban on the use of antipersonnel mines with unlimited service time. However, the world has not yet achieved this.

Scientific experiments, as a rule, are carried out in controlled conditions with more or less homogeneous soil and a relatively flat ground surface. Figs. 21 and 22 show conditions of real minefields. These circumstances need to be comprehended in further design of MW devices and algorithms for mine detection and discrimination.

Fig. 21. Minefield in the Republic of Serbska (the river bed is the mined frontline).

Fig. 22. A minefield lane in Southern Lebanon.

There are several methods for filtering out false reflections from surface irregularities. For impulse GPR with a wide operating frequency range, this problem can be solved by gating the reflected signal by range or by other methods using the high spatial resolution of broadband radars [74], [91]. However, for HSR, this cannot be used since the signal is CW or narrow bandwidth; either monochromatic [10], [88] or multi-frequency [31] which is insufficient to obtain the required range resolution. One of the possible ways to solve this problem for holographic radars is using an additional video sensor channel [92], [93].

In the first case [92], it was proposed to suppress uneven surface influence using a reconstruction method that incorporates information about the surface geometry collected by a video sensor. The microwave image was reconstructed using a modified back propagation method that incorporates a digital elevation model based on an RGB-D video sensor. The efficiency of this approach using HSR was illustrated experimentally by comparing microwave images reconstructed with the new approach with results from traditional back propagation methods in which the medium is considered homogeneous with a planar interface.

The accurate positioning of the 3-D radar was obtained with the aid of a webcam video and a graphic contrast marker (called marker AR); this solution [93] allows the acquisition on any set of points to investigate a volume. To calculate the radar position, the physical coordinates of the AR marker angles are corrected with their geometric projections on the webcam image. With the information on the 3-D coordinates of each sample, it was possible to adopt a rear projection algorithm for the reconstruction of the microwave image. By introducing the concept of augmented reality (AR) it is possible to superimpose the image of the scene on the microwave image. Thanks to the AR method of representing MW images, the need to map radar data into a reference system reported by the PC display is avoided.

The method described lends itself to various applications, the main ones being: detection of objects hidden under clothing through radar images using the portable radar scanner or representation of images from scans of non-flat surfaces (arched ceilings, columns, statues, ground natural, etc.). It should be noted that the high sensitivity of HSR to reflections from surface irregularities can also useful in applications where surface defects themselves are to be detected. As, for example, when detecting surface defects on metals [94], [95], [96].

4.2. Non-destructive testing of building structures and composite materials

Despite the fact that the first HSRs were designed with the rather narrow goal of detecting mines, particularly those with plastic cases, later work showed that they have a much wider field of applications. One of these areas is the examination of building structures in order to detect defects, embedded elements and other inhomogeneities [39], [97]. Building elements are an easier subject for scanning and interpretation since, in general, they have a relatively flat surfaces

Preprints (www.preprints.org) | NOT PEER-REVIEWED | Posted: 2 June 2021 doi:10.20944/preprints202106.0059.v1

and more or less homogeneous and predictable composition. A trained user easily learns to recognize the internal elements of a structure from a recorded MW image, and to identify anomalous targets or conditions.

The need for detecting concealed details (such as e.g. reinforcing or voids) in different structures frequently arises during repair and renovation of old buildings. Metal detectors are traditionally used to detect metallic details such as rebar, mesh, conduits or post-tensioning cables. However, the need to detect dielectric objects (e.g. plastic conduits or pipes, voids, etc.) is also of great interest and importance.

The most sensitive method, which gives information about the interior of structural elements, is based on using X-rays as the penetrating signal. However, traditional X-rays do not use backscattered signal, and therefore require a two-sided approach (with the signal source and receiver placed on opposite sides of a sounded structure). In addition, there are significant health concerns for the X-ray operator and any other nearby persons. In some important cases, both sides of a structure under investigation cannot be accessed; for example in the sounding of roadways and airstrips.

The first experiments in the field of MW imaging of structures involved concrete floor inspection as depicted in Fig. 23 [98]. The radar had multi-frequency CW signals in the range of 1.5 GHz to 2.0 GHz. The MiRascan radar was mounted on a three-wheel chassis for scanning of the concrete floor of a Moscow home prior to installation of wooden parquet. The purpose of the examination was to precisely determine the locations of plastic heating tubes in the claydite coating at a depth of 5 cm to 10 cm. A sample of the plastic tube is shown in Fig. 24. The parquet installation involves initial covering of the concrete floor/claydite screed with plywood sheets, which are held down by metal nails. These nails can inadvertently damage the pipes if their location is not known.

Fig. 23. MiRascan radar at work.

Fig. 24. A sample of the plastic heating tube.

The floor was scanned using HSR to produce the subsurface images in Fig. 25. A drawing of the tube locations was provided to the installers to prevent accidental damage. Other similar experiments are presented in [99].

Preprints (www.preprints.org) | NOT PEER-REVIEWED | Posted: 2 June 2021 doi:10.20944/preprints202106.0059.v1

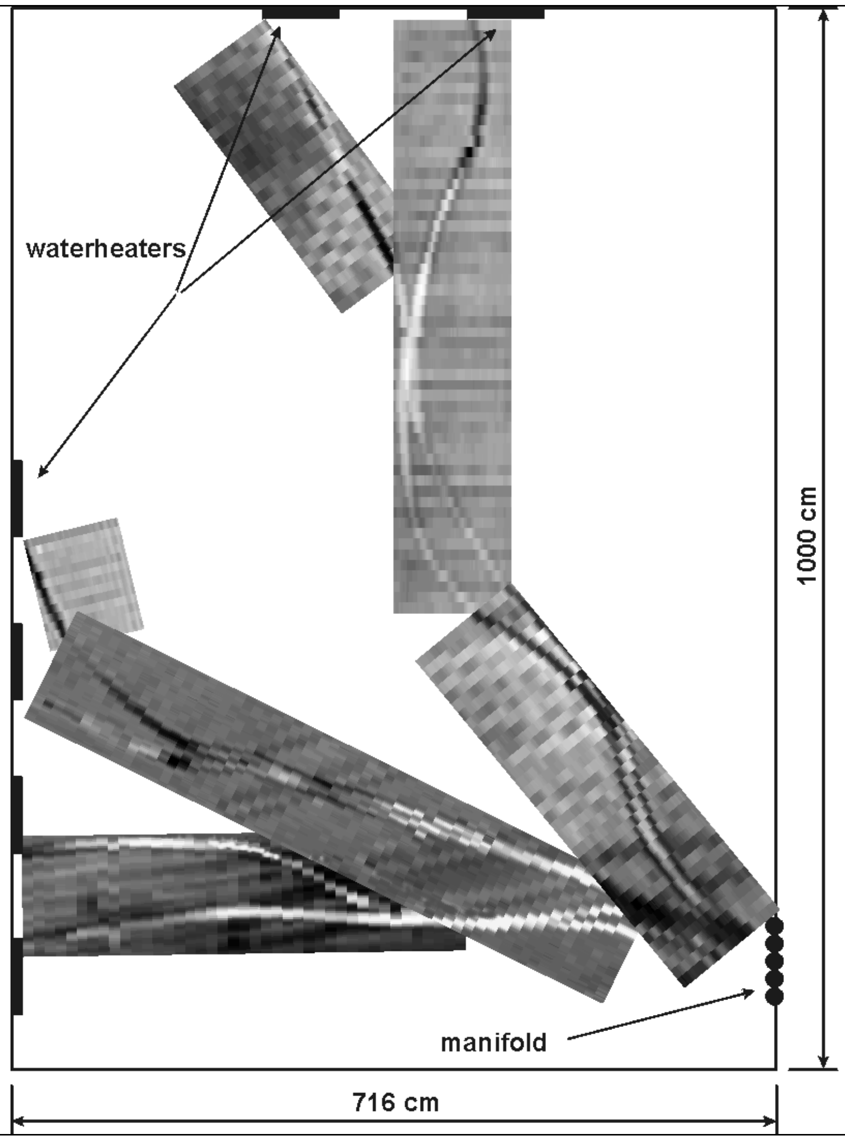

Fig. 25. MW images of plastic tubes under a concrete floor covering.

Useful new applications of HSR for non-destructive testing (NDT) arose after the catastrophic crash of the space shuttle Columbia in 2003 [100]. MW technology has proved effective for the NDT investigation of the integrity of the dielectric foamy materials used as thermal insulation of large propellant tanks, the adhesion of the tiles that are part of the Space Shuttle Thermal Protection System and other composite materials used in the aeronautical and aerospace sector; all these materials are semi-transparent in the MW range [28] and [101]. For example, consider the Shuttle's external tank which contains liquid oxygen and hydrogen propellants stored at -183 °C and -253 °C respectively. To prevent fuel vaporization and prevent surface ice formation (possibly causing damage to the space shuttle), the tank is covered with thermally insulating polyurethane foam. This layer has a thickness ranging from 25 mm to 50 mm. If the thermal insulation between the external environment typically consisting of hot and humid air and the extremely cold tank is not sufficiently, condensation of atmospheric water vapor can occur inside the cavities or porosities of the foam layer; this is a hypothesis formulated by NASA investigators after the tragic accident. The damage to the left wing of the Columbia spacecraft during the launch of the 28th mission was caused by the breaking and detachment of a piece of thermal insulation due to the sudden boiling of the water that had condensed inside the voids and which rapidly vaporized (reaching boiling point) because of the lowering of pressure with increasing altitude after launch. The effect of the damage to the thermal protection panel was manifested in the maneuver of re-entry of the Columbia spacecraft into the earth's atmosphere;

the lack of protection allowed the plasma produced during reentry into the stratosphere to penetrate and destroy the aluminum wing structure, causing the spacecraft to be destroyed. In reality, even in the previous launches of the Space Shuttles similar damage had been found, but of a reduced entity and therefore considered acceptable from the point of view of the risk for the mission [102], [103], [104]. Another cause of accidents was associated with the coating of tiles for the thermal protection of spacecraft such as the Space Shuttle; during the re-entry phase these nacelles are subjected to high thermal and mechanical stresses. A case reported in the literature [100] concerns the first flight (April 12, 1981) of the Space Shuttle Columbia where 16 thermal protection tiles were lost and 148 were damaged [100]. Even after the first and only flight of the Soviet Shuttle Buran (November 15, 1988) similar defects with serious side effects were found; in the literature [101] we report the results of the post-flight inspection which showed a partial destruction up to the complete loss of the thermal shielding tiles.

Application of MW and millimeter wave technologies for diagnostics of the heat protection shield of Space Shuttle were undertaken following the Columbia disaster [22], [28], [105]. Later, it became necessary to create specialized devices for diagnostics of products made of composite materials that are used in aerospace engineering.

As mentioned above, the newer model or RASCAN-5 radar equipped with a quadrature detector for recording signals phase and amplitude was developed to supersede the previous models which could only register amplitude holograms. This opened the possibility to design algorithms based on classical optics for the reconstruction of a microwave complex holograms [19], [20], [21].

The RASCAN-5 radar was used for diagnostic experiments on composite details [67], [68], [106]. However, these experiments showed insufficient sensitivity to small and low-contrast defects due to low operating frequencies and inaccurate positioning during manual scanning. This prompted the creation of an automated stand (Fig. 26) that would achieve the required precision [107], [108].

The experimental set-up mainly consists of a ZVA 24 vector network analyzer (VNA) with 10 MHz to 24 GHz band and a 2-D electromechanical scanner. An antenna with T_x and R_x function is connected by two flexible stable phase feeders to the VNA. The distance between the antenna and the scanning plane of the investigated object is adjusted by means of a tripod with adjustable height on which the antenna is fixed. This set-up also allowed us to experiment with different types of antennas. The measurements were carried out by moving the sample with a 2D scanner while the antenna remains fixed on the tripod. The movement system synchronized with the VNA allows to acquire the data on a programmable grid of points on the scanning area.

Preprints (www.preprints.org) | NOT PEER-REVIEWED | Posted: 2 June 2021 doi:10.20944/preprints202106.0059.v1

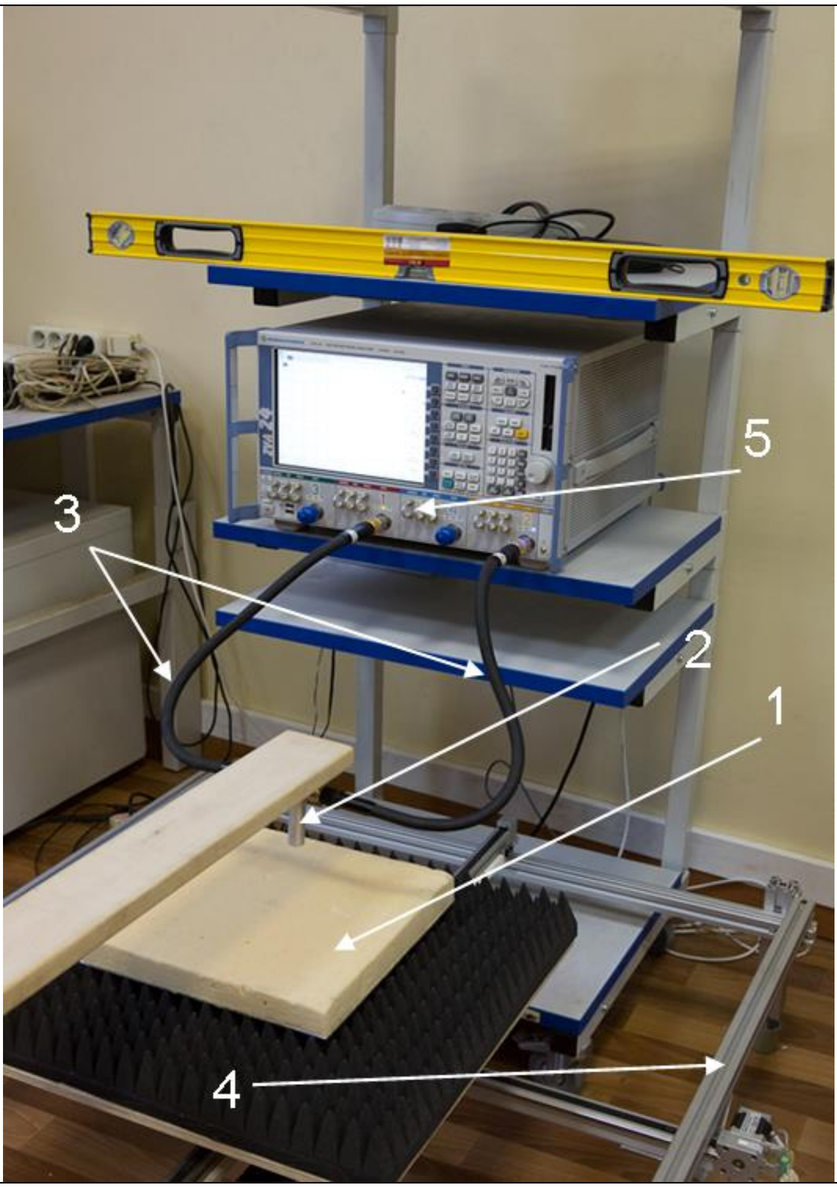

Fig. 26. Experimental high precision HST setup:
1 – test sample
2 – antenna
3 – cables
4 – electromechanical scanner
5 – vector network analyzer ZVA 24.

The capabilities of the MW NDT investigation system to detect defects of interest to the aerospace industry was evaluated using a thermal insulation sample with artificial buried defects (not visible from the outside). This sample was made by a Russian aerospace company whose mechanical design is shown in Fig. 27. The sample area 500 mm x 400 mm and the thickness of the thermal insulation (polyurethane) equal to 40 mm. This insulating layer is fixed to a 5mm thick aluminum plate by gluing. The sample preparation phases are as follows: in the first phase the adhesive was sprayed onto a central circle with a diameter of 270 mm and subsequently three circles with a diameter of 50 mm and a height of 1 were removed by cutting on the lower surface of the insulation layer. The centers of these three circular defects are equally spaced at an angle of 120° (see Fig. 27).

Preprints (www.preprints.org) | NOT PEER-REVIEWED | Posted: 2 June 2021 doi:10.20944/preprints202106.0059.v1

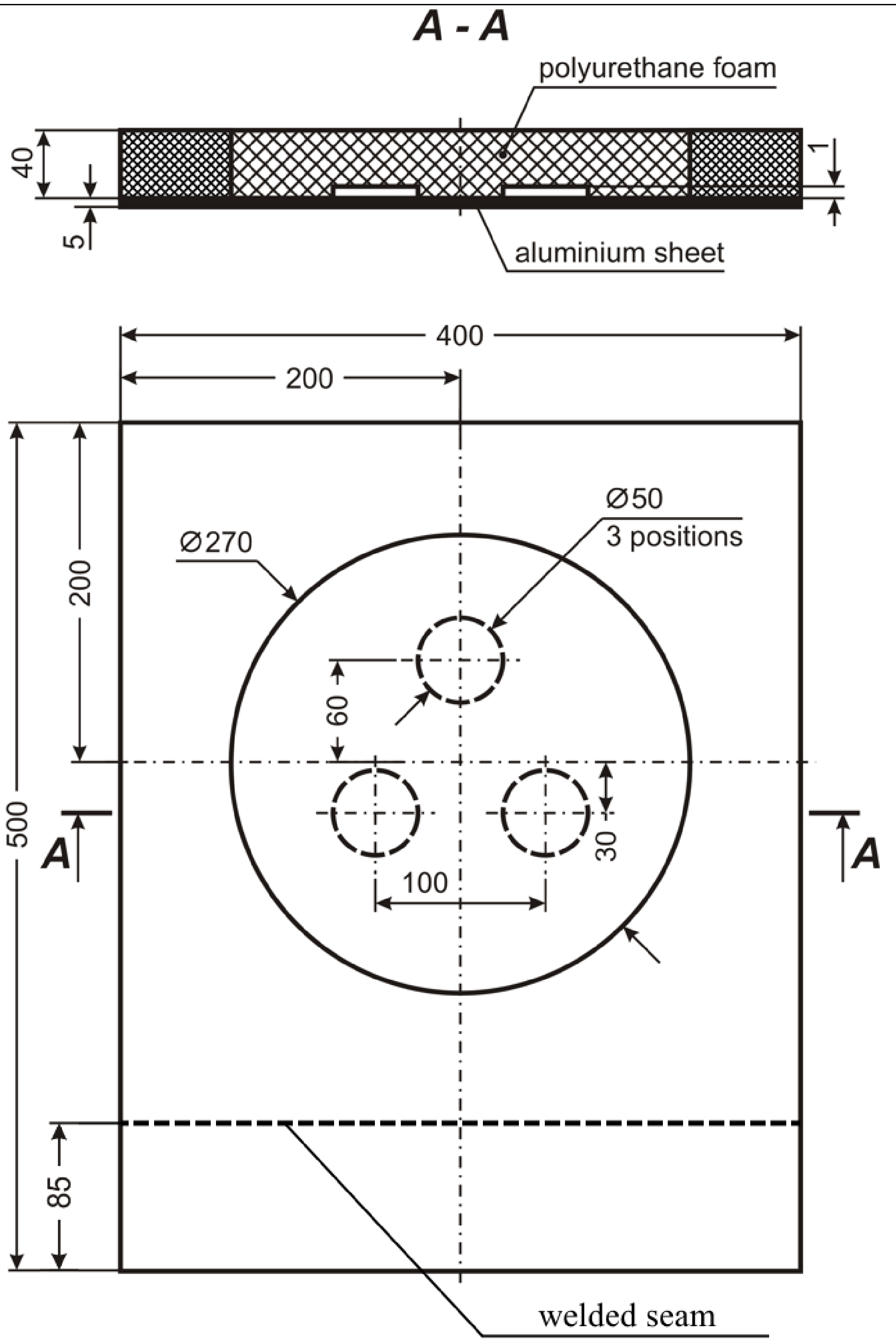

Fig. 27. Mechanical drawing of the polyurethane insulation sample with three artificial defects

Therefore, in the sample there is no adhesion to the aluminum plate on the surfaces of the three buried circular defects ("blind defects) while the deposition of the glue on the circular surfaces of the cuts has been preserved to simulate the effect of delamination at the interface between the foam and metal. Consider that the thickness of the primary coating and of the glue is about 200 µm. In the second step, the volume of the sample was filled with foam.

Finally, to evaluate the different defect detection capabilities, scans were carried out with the HSR at three frequencies of 7 GHz, 15 GHz and 22.5 GHz, as reported in Fig. 28 [109]. As foreseen by the theory, the spatial resolution improves with increasing frequency but consequently increases the attenuation with possible effects on the contrast of the image. At the frequency lower than 7 GHz, it is not possible to detect the three defects in the polyurethane foam layer, while they are detectable at the higher frequencies equal to 15 GHz and 22.5 GHz. Always at the higher frequencies the alloy weld bead. The 7 GHz scan does not clearly detect all these details and is affected by reflections from the outer edges of the metal plate. By applying the reconstruction algorithm to the scan data at 22.5 GHz, a strong suppression of edge effects is obtained, as these signals do not contribute to the formation of the interference pattern which is the basis of the holography principle. It is interesting to note the presence of other information in the same radar image, indicated with labels n.1 and n.2 in Fig. 28. These are real defects generated during the preparation phases and not artificially produced. This case study testifies that the manufacturing procedures, even if carried out by qualified personnel and in specialized laboratories, are not free from defects that can be detected by HSR scans with high frequency.

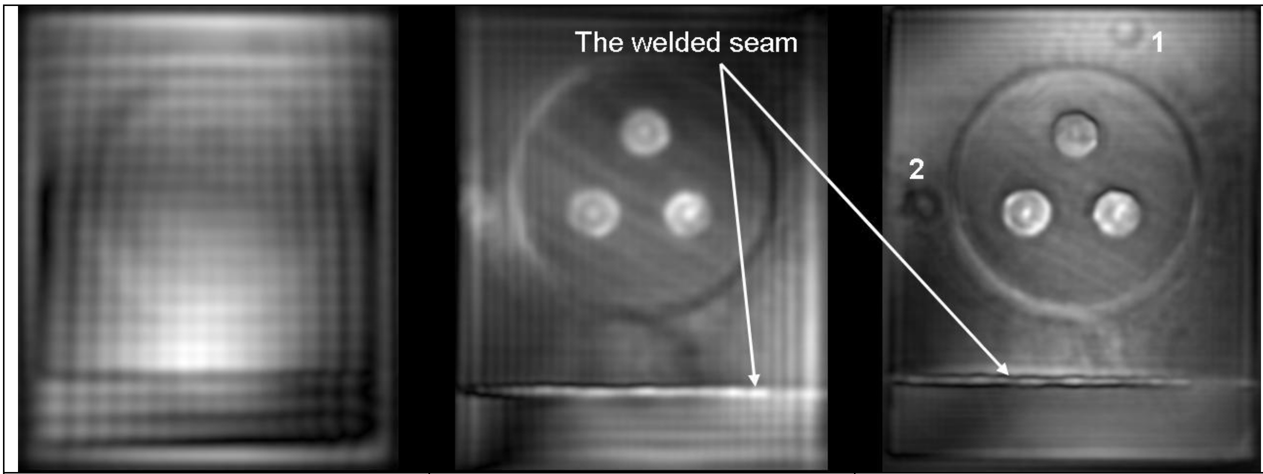

7 GHz (λ≅4.3 cm)	15 GHz (λ≅2 cm)	22.5 GHz (λ≅1.3 cm)

Fig. 28. Results of the sample examination at three different frequencies.

This technique was also used for experiments with a sample that was submitted for examination by the Vikram Sarabhai Space Center, India. Similar blind experiments again validated the technology [110]. There are other applications that include detection of water intrusion in honeycomb composite products [30], [111], diagnostics of tube coverings [112], [113], [114] among others.

Although HSR technology is not yet widespread in the field of non-destructive testing for the investigation of materials and dielectric components, there are concrete examples that show clear advantages in the aerospace industry. Being able to compare HSRs with ISRs, we can meanwhile affirm that the former is cheaper and more adaptable to the conditions of use. HSR technology can also be compared with traditional ultrasonic NDT techniques applied limited to dielectric materials such as thermally insulating polyurethane foams with high porosity, thermal protection tiles made with sintered quartz fibers and composite materials based on fiber glass or carbon with a honeycomb structure: all of these materials or components exhibit high attenuation for acoustic waves [27] at frequencies such as to provide a spatial resolution comparable to MW HSR systems, [115]. Furthermore, ultrasonic systems are efficient when the transducers are placed in contact with the surface to ensure a good mechanical coupling, often reachable only by using coupling gels or liquids.

Preprints (www.preprints.org) | NOT PEER-REVIEWED | Posted: 2 June 2021 doi:10.20944/preprints202106.0059.v1

4.3. Cultural heritage inspection and diagnostics

This section is a partially a continuation of the previous one, but takes into account the specific requirements and precautions when examining important artworks, architecture, and other cultural heritage objects. This is where the advantages of various NDT methods are most manifest. Traditionally, several NDT methods have been applied to these studies, with the selection and effectiveness of a particular technology dependent upon the properties of medium under investigation. To assess the capabilities of different NDT for cultural heritage studies, additional research was done; see for example [116].

One of the first examples of the use of HSR in an historical building was during the reconstruction of the early 19th Century Senate building in Saint-Petersburg, Russia [37]. The building was being refitted for using it by the Constitutional Court of Russian Federation (Fig. 29). The building was built by the Russian-Italian outstanding architect Carlo di Giovanni Rossi in 1829–1834 and has great value for Russian culture. An in-floor water heating system had been installed previously, but with the arrangement of pipes not documented. In addition, there are electricity and communications cables as well as metal mesh under the concrete floor of the building. Workers wished to avoid damaging pipes and cables during the installation of parquet as described in the previous section. In this construction, first, metal mesh with 150 mm spacing had been laid on the concrete subfloor. Then, pipes were fastened to the mesh by the plastic clips. Various types of pipes had been used including cross-linked polyethylene (PEX), multi-layer (a composite of aluminum and PEX) and polybutylene (PB). The spacing between pipes was about 30 cm. The pipes were then covered by a cement screed with thickness above the pipes of about 3 cm.

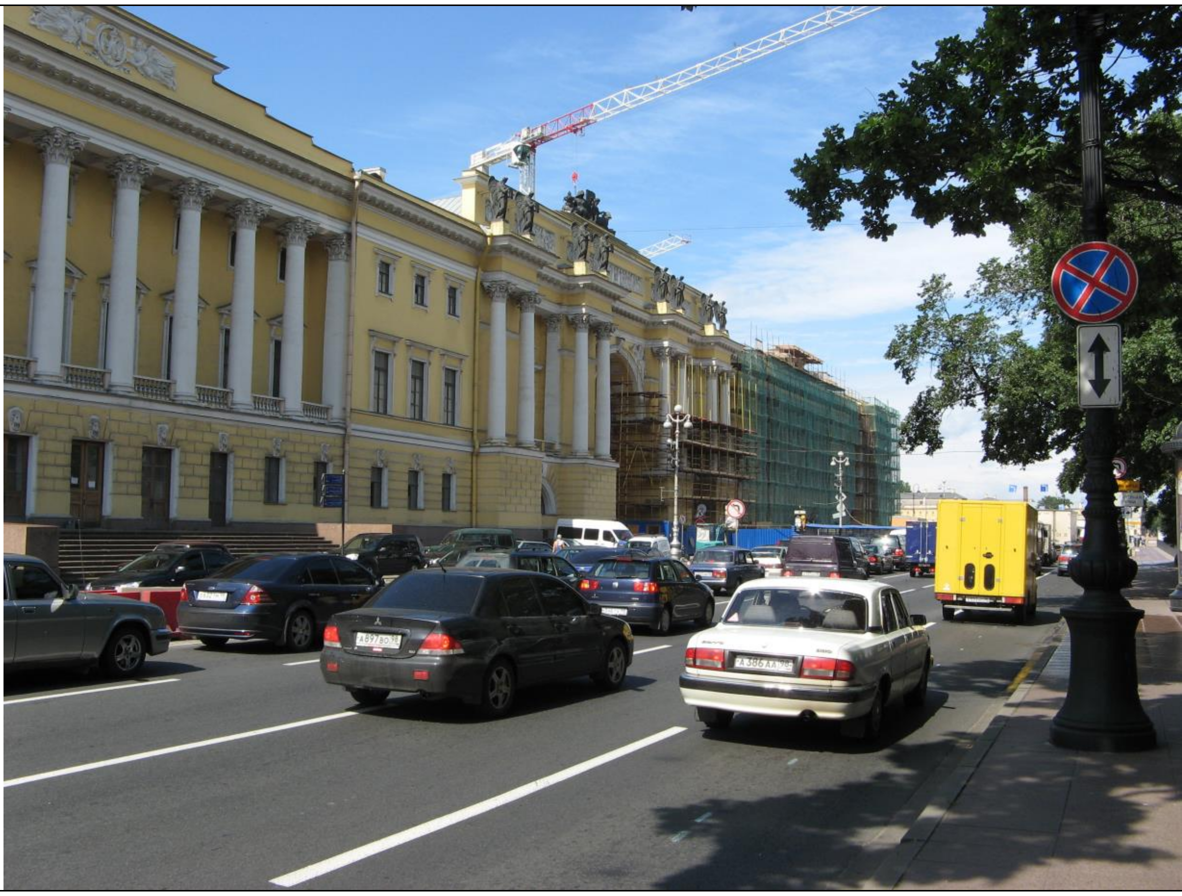

Fig. 29. Senate building during the time of reconstruction work.

There was concern that the plastic pipes would be invisible against the background of the highly MW reflective metal mesh. However, there are several reasons (effects) that facilitate this

Preprints (www.preprints.org) | NOT PEER-REVIEWED | Posted: 2 June 2021 doi:10.20944/preprints202106.0059.v1

task. Recall that the contrast of an object on an HSR image depends on its reflectivity and the phase shift which is a function of the distance from the antenna aperture to the target. For elongate objects radiation polarization also has strong influence on the recorded contrast.

The work of floor inspection was carried out with the aid of a RASCAN-4/2000 holographic subsurface radar with discrete CW operating frequencies in the range of 1.6 GHz to 2.0 GHz (Fig. 30). The total area of the scanned surface was 16.7 m^2. Fig. 31 depicts a portion of the scanned floor area. As expected, there was no contrast between pipes and metal mesh in the parallel polarization radar images. But in the cross-polarization radar images, the plastic pipes were clearly visible. A detailed radar image showing pipes bending as they cross a cable is shown on Fig. 32.

Fig. 30. RASCAN-4/2000 radar.

Fig. 31. Part of scanned area floor.

Fig. 32. MW image presents pipes that bend around a cable.

As the survey progressed, the operator analyzed the image and drew the results in chalk on the floor. The traces of heating tubes were marked in blue chalk, while red chalk was used for cables as in Fig. 31. The composite MW image of the total scanned area is presented in Fig. 33a. The layout of the heating pipes according to the received images is shown in Fig. 33b.

Another application concerns the scanning of a marble medallion in the floor of the Temple of San Biagio in Montepulciano, Italy (see Fig. 34) [36]. From a-priori information on the typical thicknesses of such marble medallons, it was decided to scan with HSR at 4 GHz with RASCAN-4/4000; the holographic images show a complex internal structure, as shown in Fig. 35. It is also possible to notice a good spatial correlation between the optical image and the HSR RASCAN images. With reasonable certainty, we could conclude that the objects highlighted by the contrast patterns are dielectric and non-metallic materials. Below are the interpretations for the three contrasting patterns shown in the yellow squares in Fig. 35. In the vertical squares (n.1 and n.2 in figure 35) they can represent the presence of bricks or wooden supports under the marble medallion. Furthermore, the multi-frequency images can be viewed in sequence by an application of the Rasan software suite: with the video (attached as a multimedia file to the article) it is noted that there is a gradual shift of the contrast patterns, and this effect is typical of RASCAN HSR images obtained from a curved surface. Therefore, on the underside of the marble medallion, there may be a curved vault above a void or opening. The third contrast pattern in the RASCAN radar image (inclined yellow square n.3) corresponds to a thin line on the marble visible in the optical image shown on the right in Fig 35. Since the dimensions of the crack are much smaller than the length of wave it is assumed that this response is due to the presence of humidity. Cuts on marble slabs filled with water and then joined again confirmed this hypothesis [36].

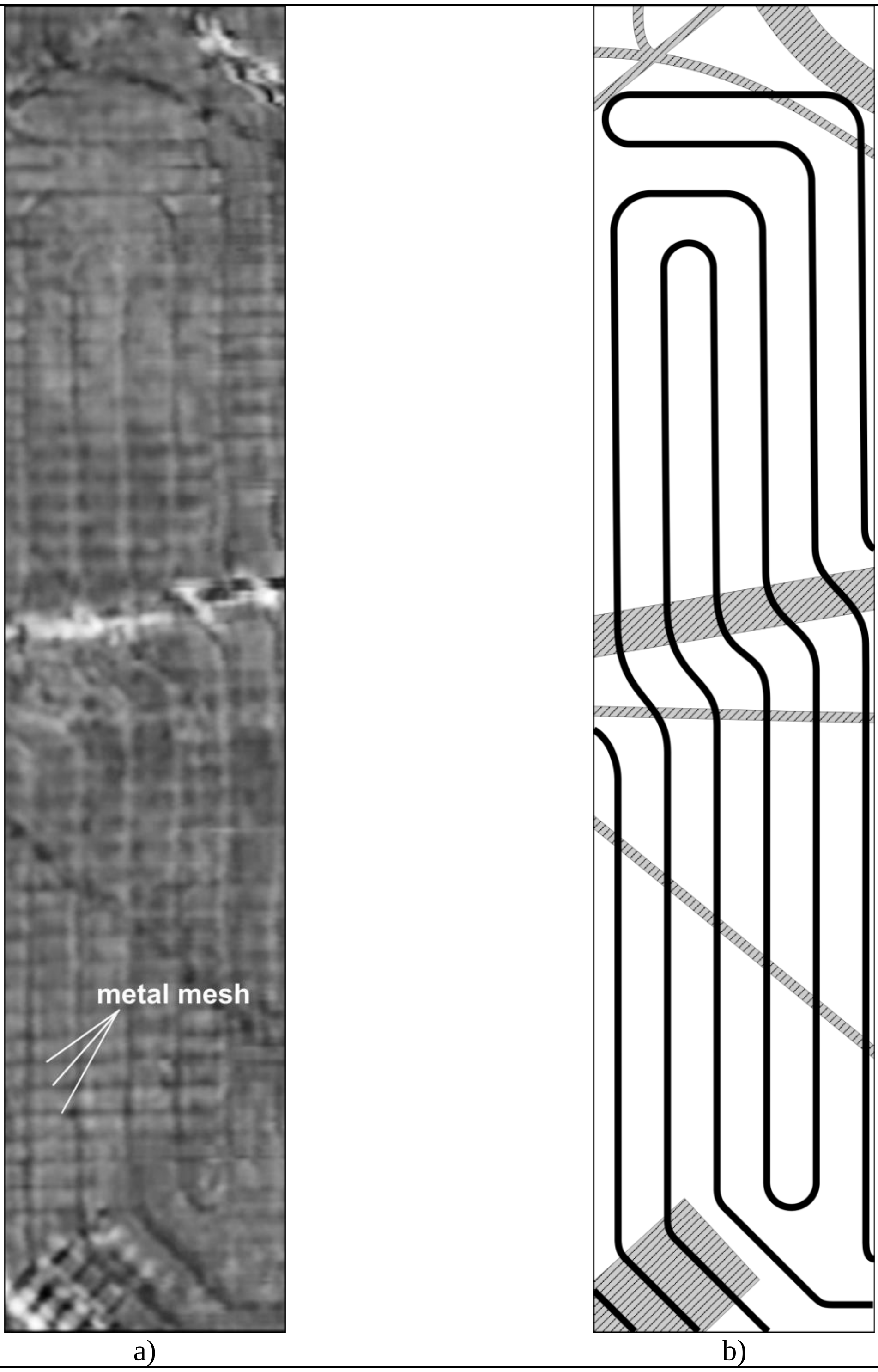

Fig. 33. Radar image of total scanned area a) and layout of heating pipes beneath the floor b).

A detailed historical research in the church archive indicates that the medallion was placed around 1590 during the funeral ceremony of a Prelatio of the Casata Cervini family. The current burial place of the Prelatio is not registered. However, the hypothesized supports and the arched vault suggest the possibility that under the medallion there could be the remains or relics of the Prelatio.

Preprints (www.preprints.org) | NOT PEER-REVIEWED | Posted: 2 June 2021 doi:10.20944/preprints202106.0059.v1

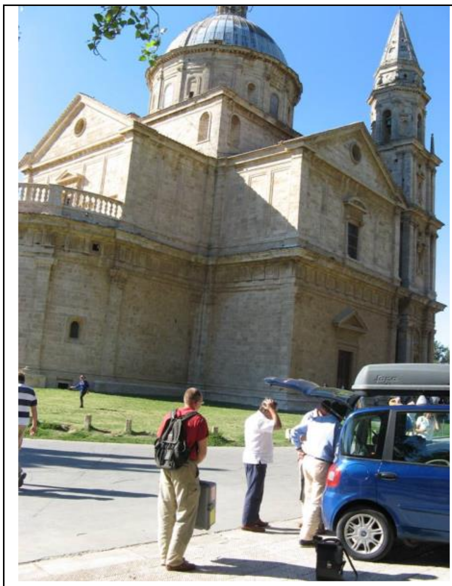

Fig. 34. Temple of San Biagio in Montepulciano, Italy.

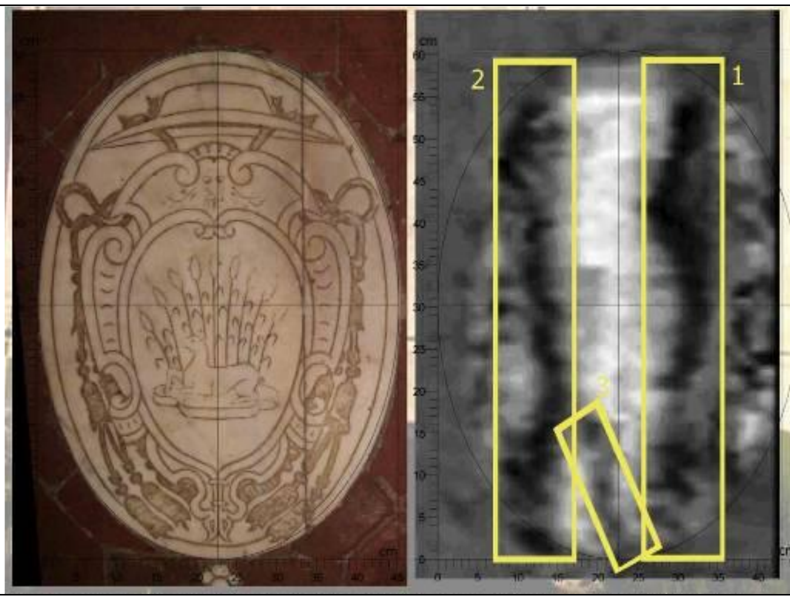

Fig. 35. Visual and MW images of marble medallion.

Other examples of cultural works that can be studied by HSR are the mosaics and frescos that decorate many buildings of historical importance. The preservation and maintenance of these valuable decorations are dependent upon identifying possible hidden problems or conditions. The choice of the appropriate technique or combination of different NDT techniques depends, in general, on the depth of investigation, the resolution, the possibility to have direct contact. One of the possible devices that could be useful for this goal is HSR [117]. Fig. 36 demonstrates the application of RASCAN radar in the investigation a wall mosaic in La Martorana Donazione church, Palermo, Sicily by Padua University researchers.

Fig. 36. RASCAN radar in use during investigation of a wall mosaic in La Martorana Donazione church, Palermo, Sicily.

An example of non-destructive investigation with HSR concerns the Croce di San Marco which dates back to the mid-fourteenth century and is attributed to Puccio di Simone [118] and considered one of the masterpieces and greatest examples of Florentine painting: the dimensions of the cross are imposing reaching a height of 6.3 meters. The cross was assembled by the masters of the time by composing perpendicular axes with a retractable joint. The thickness of each poplar board is 7 cm and the entire structure, including the crossbars, reaches a thickness of about 25 cm with an estimated total weight of around 500 kg (see Fig. 37).

Fig. 37. The Cross of San Marco

In the first phase of investigation, it was decided to scan with RASCAN HSR three areas covering the supporting infrastructure and the area of the relief insert for the aureole, Fig. 38. The artwork was protected by a green cloth supporting a plexiglass sheet marked with parallel and numbered scan lines.

The first scanning area is positioned vertically along the trunk of the image. In the images from the three intermediate frequencies at cross polarization, metal nails are clearly visible, and may be intended to hold the wooden planks together. In cross polarization, the image at a frequency of 3.7 GHz clearly shows the contrast between areas laminated with gold leaf (bright in Fig. 39) versus those where the wood is painted (darker in Fig. 39). In addition, there is a dark curved shape associated with blood emanating from the wound on the side of the Christ figure (compare Fig. 37 with Fig. 39 right (cross polarization).

The second area of interest was chosen at the top of the cross just below the halo. Also, in this scan the metal nails are clearly detected, especially in the image obtained from the channel with parallel polarization antenna. In this case, the lines of the manual scan were performed in an orthogonal direction with respect to the previous case. At the three highest frequencies, both in cross polarization and in parallel polarization, numerous streaks compatible with the wood grain are visible. The anisotropic of the dielectric constant due to the fibrous nature of the wood explains this high sensitivity of the HSR images to the characteristics of the investigated dielectric medium. Finally, the third scan area was placed overlapping the first, but narrower and higher, rising above the halo area.

Fig. 38. Examination of the Cross of San Marco with holographic radar RASCAN.

In the analysis of the HSR images we found a peculiarity that needs a more explanation: it is the presence of a shape that copies the representation of the gush of blood that comes out of the wound on the chest of Jesus Christ (see Fig. 39). This contrast pattern was not expected as it is superimposed on the gold leaf that surrounds the martyr's body. As it is not plausible that a dielectric layer less than a tenth of a millimeter thick could modify the amplitude or phase of the reflected wave, an explanation was sought by designing a dedicated experiment in the laboratory of the Opificio delle Pietre Dure in Florence. To recreate this phenomenon, a specimen was made with gold foil partially covered with a layer of red lead paint. As expected, the area covered by the layer of red lead is indistinguishable from that on gold foil without lead. A plausible hypothesis is that the paint used for the blood contains a metal component (possibly zinc), and therefore can be modelled as a non-perfect conductor. In this case the electric field would be cancelled only partially, thus determining a phase variation different from 180 °, resulting in the image on the right of Fig. 39. This hypothesis was confirmed by a chemical analysis carried-out previously by the Opificio delle Pietre Dure of Florence, which detected high levels of lead in the paint used to depict the blood. Somewhat surprisingly, lead was used at the time creation of this piece to make the colour white. Here it may have been used to create the appearance of the flow of blood by making striations of red and lighter red to white.

Preprints (www.preprints.org) | NOT PEER-REVIEWED | Posted: 2 June 2021 doi:10.20944/preprints202106.0059.v1

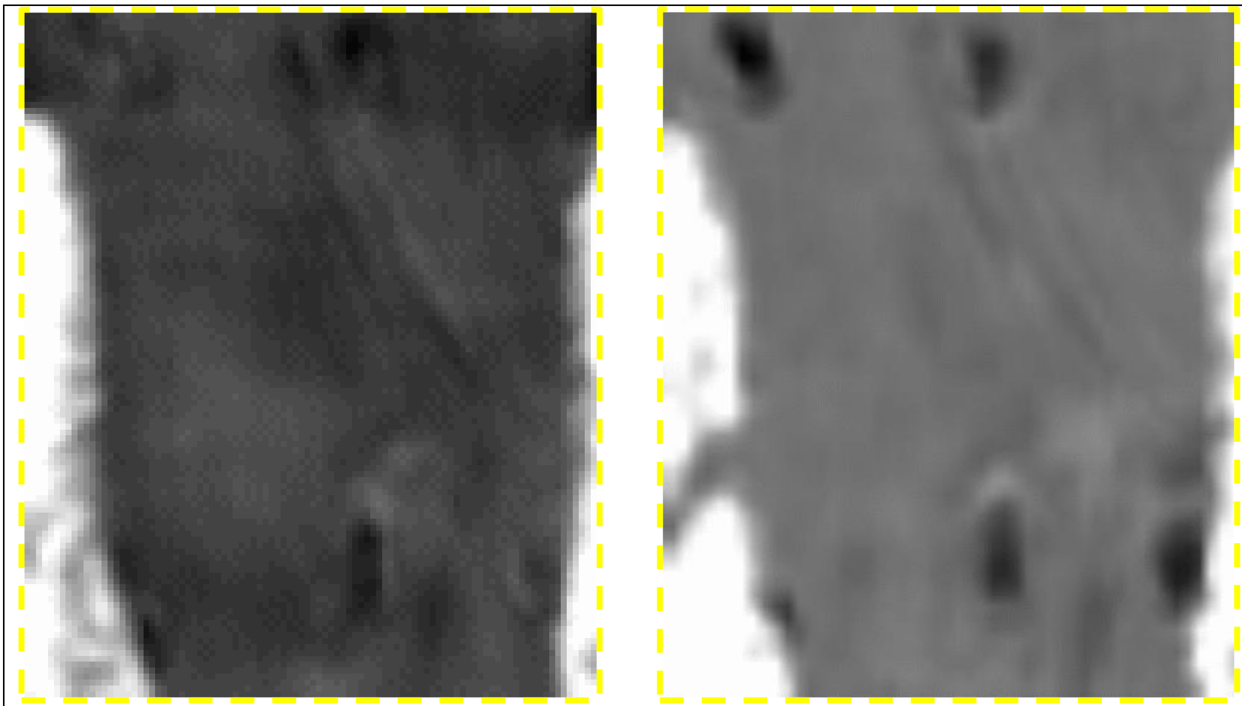

Parallel polarization Cross polarization

Fig. 39. HSR images of the Cross of San Marco recorded at 3.7 GHz.

In the USA, termites and other wood boring organisms inflict $4.5 billion worth of damage on homes and other buildings each year. While professional inspections, trained dogs, and CO_2 detectors can spot active colonies, the old damage from previous infestations is often not visible at the surface of wooden structures. HSR of the RASCAN type has been shown to be effective in detecting hidden tunnels and other damage [54]. Fig. 40 shows a wooden beam in a structure on the former estate of US President James Buchanan (1791–1868). On the left is a photo of the surface of the old beam. The center is an HSR image at parallel polarization and 3.7 GHz signal frequency. The dark contrast highlights its joint with an adjacent beam to the right, as well as an area with no obvious surficial manifestation. The photo on the right shows termite damage exposed by peeling away the surface of the wood.

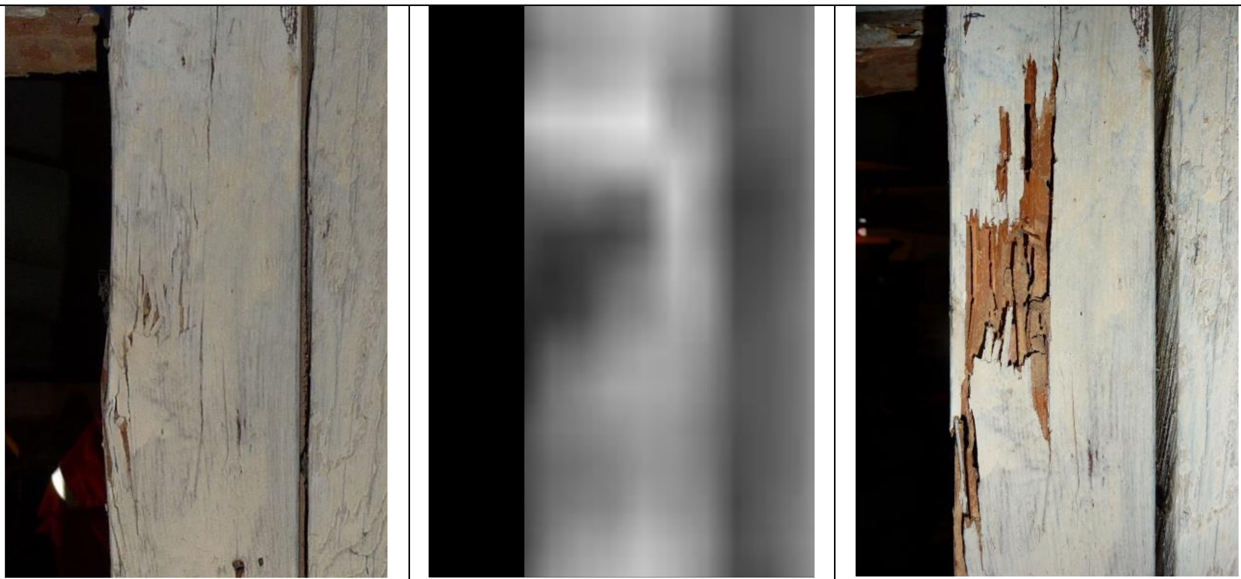

Beam in historic structure HSR image at 3.7 GHz Insect damage revealed

Fig. 40. Wooden beam in historic structure with insect damage detected and revealed.

Preprints (www.preprints.org) | NOT PEER-REVIEWED | Posted: 2 June 2021 doi:10.20944/preprints202106.0059.v1

Perhaps the most exotic application of holographic radar has been for the detection and imaging of hidden dinosaur tracks [119], [120]. The study of dinosaur tracks, (shape, depth and distance between the footprints in sequence) provides important information about these prehistoric animals, in particular regarding their dynamic behavior, which is often not revealed by the fossil remains. Dinosaur tracks are commonly preserved as paired molds and molds that can separate to reveal the print. These footprints were formed when ancient animals stepped on soft ground leaving footprints. If the sediment fills the series of footprints before they are eroded by the elements (wind, water, etc.), then the track could be fossilized and preserved for millions of years. Until now, dinosaur tracks have been studied when they emerged from the ground by removal of the surface layer or removed from the rocky area and kept in laboratories or museums. Where these are exposed, it is reasonable to assume that other tracks exist, but they are covered by younger rock layers and hidden from direct observation. Following partially successful laboratory and field experiments, it was proposed to use the high precision experimental installation shown in Fig. 26. These experiments were conducted in three frequency ranges: 6.4 GHz to 7.0 GHz, 12.8 GHz to 15.2 GHz and 18.0 GHz to 21.5 GHz. A cast and modeled dinosaur trace model was created by making a plaster cast of a real dinosaur trace (var. Anamoepus [121] from Dinosaur State Park in Connecticut, USA) and reproducing the well-fitting mold from this cast as shown in Fig. 41. The half of the specimen with the impression mold has an area of 255 mm x 225 mm and a height of 27 mm. The cast sample has the same area, but 22 mm high. The footprint is located in the center of the samples and has dimensions of 11 cm in length by 7.5 cm in width.

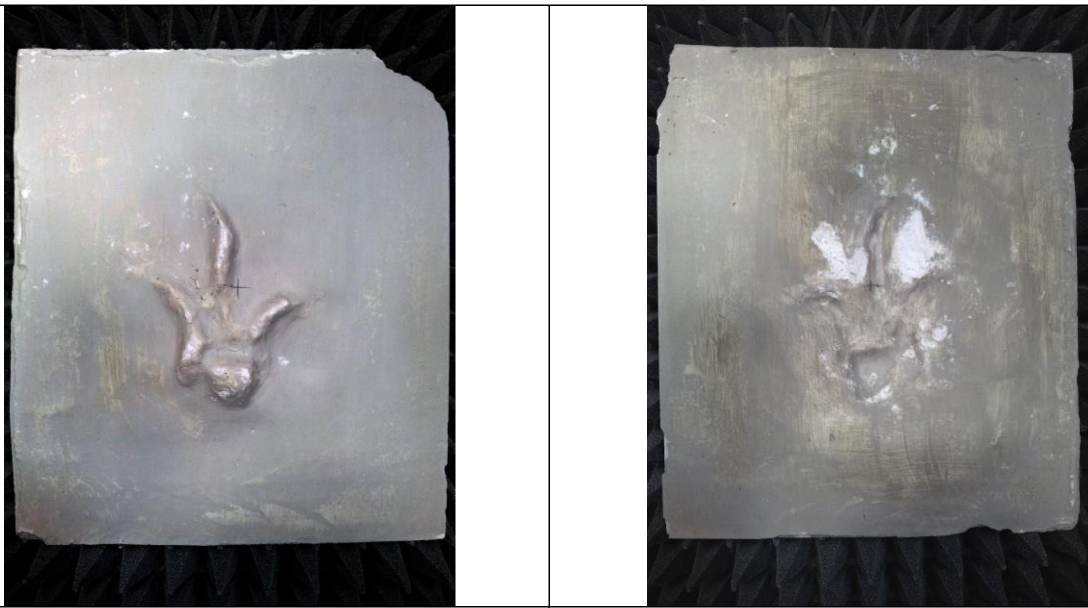

a) b)

Fig. 41. Cast (a) and mold (b) of *Anamoepus* dinosaur footprint.

Experiments with only the cast or mold with clean plaster surfaces conducted in all frequency bands showed clear radar images that gave better results at higher frequencies. From this experimental investigation and from the support of the simulations of digital fingerprint models, we can believe that the MW holographic microwave radar is suitable for performing non-contact scans of areas in which the traces are even partially exposed. The ability to scan without contact is an important advantage considering the fragility of the thin layers that covers the sequences of the impressions, and the difficulty of recording and reproducing them digitally when they have very low relief. To highlight the ability to discover hidden footprints, the mold of the implant was coupled with the plaster cast to reproduce the experimental situation in nature. This imaging was most successful when the mold and cast were separated by a very thin (less than 1 mm) slip of clay (as is common for real tracks).

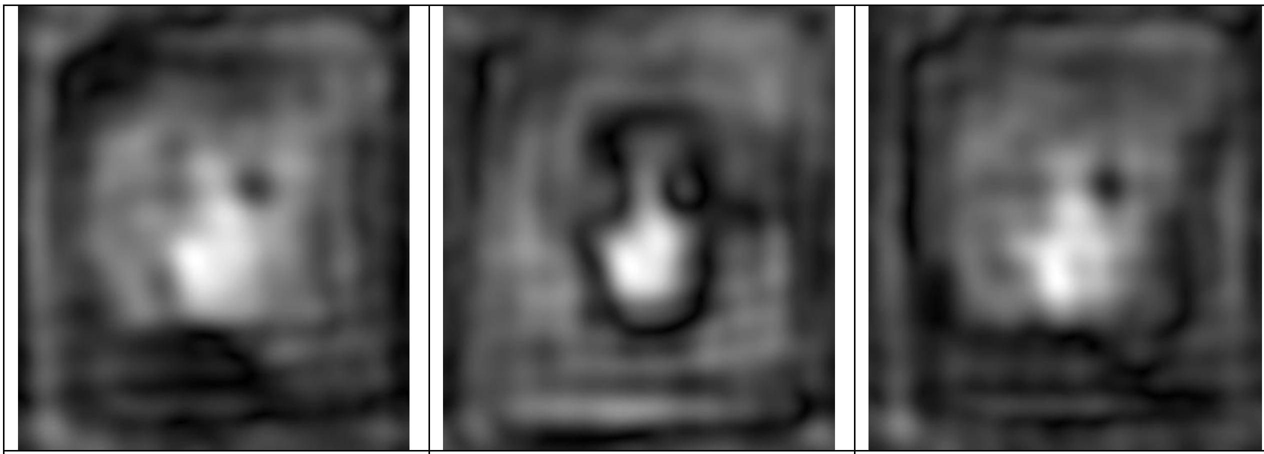

a)	b)	c)

Fig. 42. Reconstruction of holograms registered at 7 GHz of the samples:
a) Mated clean surfaces of the samples
b) Mold sample surface covered with sand
c) Polyethylene sheet separating the surfaces between mold and cast.

In the final experiments with the high precision setup, some amount of sand was dusted onto the surface of the mold to simulate delamination of the layers which is typical for real footprints — especially those prone to separation to expose and reveal the track. The contrast of the hidden footprint was increased and became comparable to that for the uncovered mold half. This occurs by introducing a dielectrically contrasting air gap between the samples (similar to the clay slip in previous experiments). Results of the high precisions experiments are presented in Fig. 42.

Other experiments that used RASCAN HSR on paleontological samples include a case where images were made of a partially concealed rostrum of an Upper Jurassic to Lower Cretaceous fossil crocodylomorph beneath the upper surface of a 21-mm thick limestone slab from the Maiolica Formation. The specimen, recovered in the Altopiano di Asiago (Vicenza Province, Italy), is presently housed in the paleontological collections of the Rovereto Civic Museum (Trento Province, Italy). The holographic radar response recorded on the surface where the fossil cannot be observed correlates well with the actual fossil shape revealed on the reverse side of the slab. This study was done using a RASCAN-4/7000 HSR radar with discrete signals at frequencies between 6.4 GHz and 6.8 GHz. These frequencies easily penetrated several centimeters of the limestone. The radar has receiving antennas with both cross and parallel polarization relative to the transmitter. As in many previous examples, on a radar plan-view image, objects can often be identified directly by their shape. Results of the experiments presented in Fig. 43 [40].

The results of these paleontological experiments are not fully developed, but this is a very new field of application for HSR. Therefore, further field trials are needed to understand the relevance of the microwave holographic technique for the remote detection of characteristic shapes in areas of paleontological interest. For example, the high dielectric contrast sensitivity of the proposed method has been exploited for imaging hidden invertebrate fossils that have been pyritized or otherwise replaced by secondary minerals with very different dielectric constants from the rock in which they were fossilized.

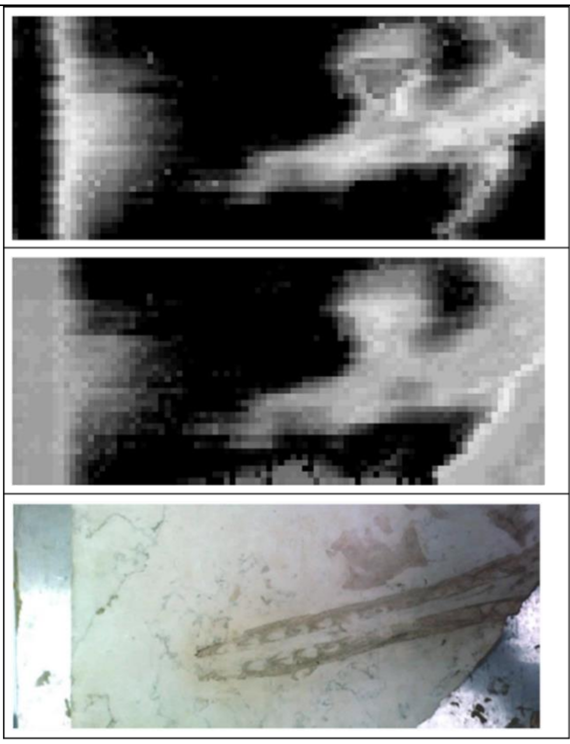

Fig. 43: The image is the summed modulus of scans 6.7 GHz parallel and 6.7 GHz cross polarizations (top). The image is the full summed modulus of scans 6.4, 6,5, 6.6 and 6.7 GHz parallel and cross polarizations (centre). A photograph of the lower side of the limestone slab roughly aligned to correspond to the scan area (bottom).

It is worth mentioning in this section a recent discussion to use MW for non-destructive investigation of Egyptian pyramids [38]. The study of ancient Egyptian monuments has always attracted the attention of scholars from all over the world (see Fig. 44). An example of this interest is evidenced by the discovery of hollow volumes inside the Great Pyramid of Giza (or Pyramid of Cheops) using special muon sensors (see Fig. 45) [122]. The validation of this discovery is difficult as it requires perforations of the pyramid, therefore a highly destructive and expensive technique. Validation by another non-destructive method was then proposed to confirm this finding and provide an equally accurate assessment of the position and shape of the discovered cavities. Following a review of the literature on the different methods used in the evaluation of cultural objects, a preliminary theoretical and simulated study was made for the application of the microwave holographic technique to detect cavities or other unknown structures of interest to archaeologists / Egyptologists and certainly for the general public interested in ancient Egypt.

Fig. 44. Photo of the Sphinx with the Khufu's Pyramid in the background.

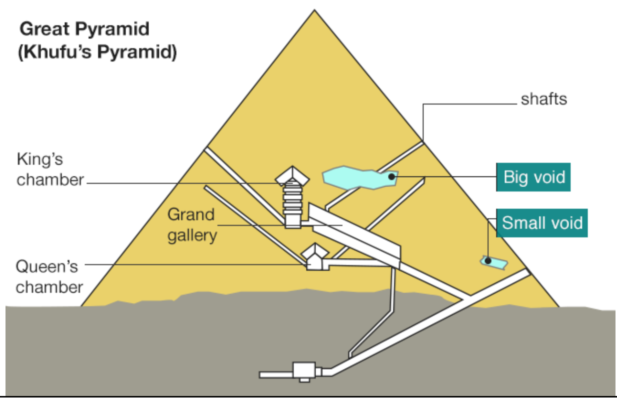

Fig. 45. The estimated locations of the Big and Small voids detected by muon tomography [122].

Based on the analysis of the range of possible electromagnetic properties of the pyramid, a simple numerical model was constructed which allowed evaluation of the possibility to detect voids in the Great Pyramid using electromagnetic radiation at a frequency of 100 MHz, corresponding to a wavelength in air of about 3 meters. The frequency of 100 MHz selected for calculations is to some extent a compromise because, with increasing frequency the attenuation and reflection of the signal at small inhomogeneities increases, and at lower frequencies the spatial resolution suffers. Since the exact geometric dimensions and forms of the voids indicated by the muon experiment are unknown, the void in the pyramid was modeled using an elongated ellipsoid of revolution with size D = 30 m along the longitudinal axis and d = 5 m along two other transverse axes.

Fig. 46 represents the influence of the polarization direction on form and amplitude of recorded signals for a case when an electromagnetic wave input from one side of the pyramid scatters on the void and is recorded on another side. The polarization angle of the electromagnetic wave is measured from the major axis of the ellipsoid. As seen from this figure, at polarization angle of 0º, i.e. parallel polarization, the recorded signal is noticeably stronger than at perpendicular one at angle of 90º. This effect could give additional information about internal objects in the pyramid [38].

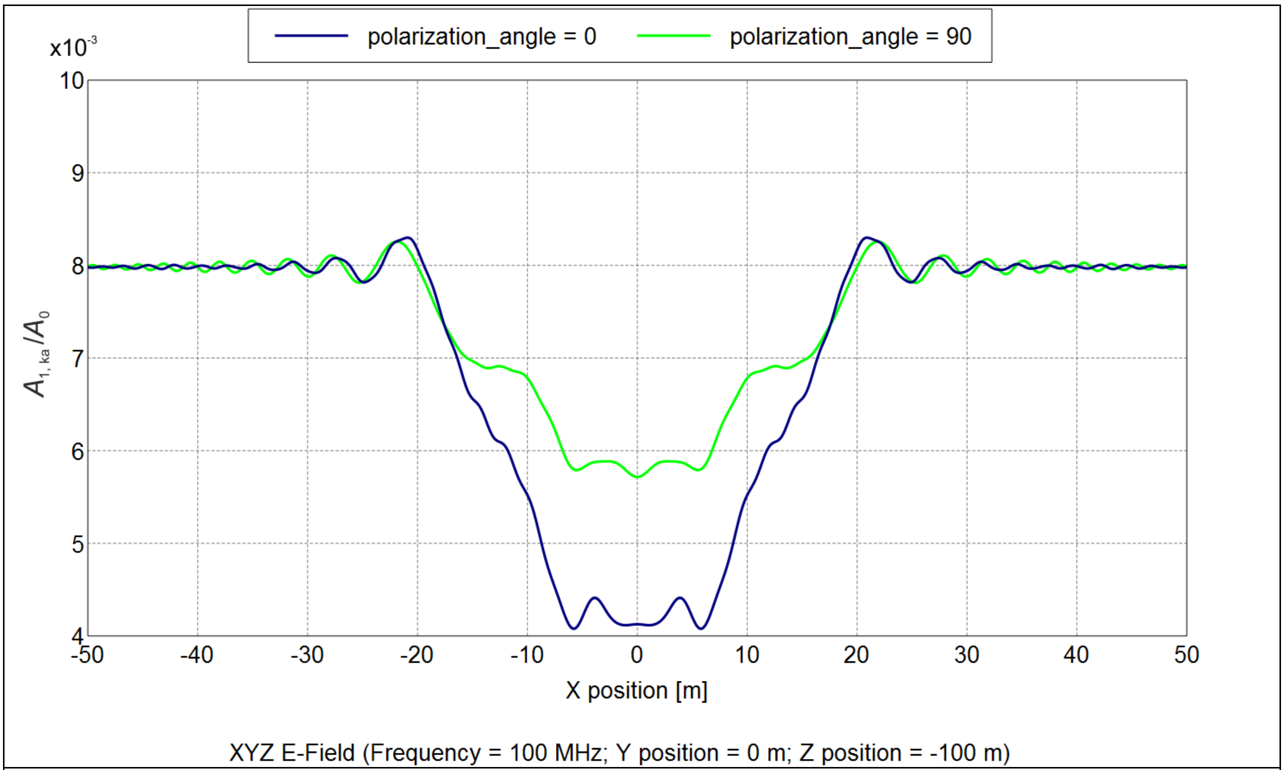

Fig. 46. Influence of wave polarization direction on the form of recorded signals.

A better result and more information about internal structure of the pyramid could be obtained if the inverse problem could be solved — i.e. reconstructing the void geometry from the recorded scattering. As the calculations show, the level of signal attenuation in the pyramid body is also essential for solving the problem. Estimates were made of the possible values for the attenuation coefficient at which reception of radio waves passing through the pyramid would be possible considering the intrinsic noise of the transceiver system, as well as external electromagnetic noise [38]. The proposed method of radar imaging of lossy inhomogeneous media could be used at other historical sites less voluminous than Khufu's Pyramid. Examples of such objects are stone fortress or monastery walls, or any ancient buildings or masonry structure with thickness of more than 1.5 m. Another possible subject for HSR imaging, which is well

Preprints (www.preprints.org) | NOT PEER-REVIEWED | Posted: 2 June 2021 doi:10.20944/preprints202106.0059.v1

known in the world, and surrounded by many mysteries and legends, is the Egyptian Sphinx, Fig. 44.

4.4. Monitoring of human vital signs

There is keen interest in using MW methods for medical diagnostics and imaging, and emergency response such as detection of living persons beneath rubble or behind walls. In the latter applications, by subtraction of signals reflected from motionless objects it is possible to achieve highly sensitive detection of moving surfaces or reflectors such as the rise and fall of a breathing person's chest. According to estimates available in the literature, the sensitivity of this method can achieve 10^{-9} m [123]. Although there are many potential moving targets that could be detected, this section focusses on detection and diagnosis of living persons.

Organs in the human body that display periodic fluctuations are primarily the heart and lungs. Their movements depend upon both physical and mental state, but generally have frequencies in range of 0.8 Hz to 2.5 Hz for heart and 0.2 Hz to 0.5 Hz for lungs and are quasiperiodic. Remote or contactless measurement of respiration and pulse rates of a person, whether in line-of-sight or concealed, were the focus of MW research [49][56], [57], [124], [125], [126]. Measurement of breath and pulse signals required development of a sufficiently sensitive radar and development of algorithms to suppress extraneous background reflections in order to reveal the time-varying biological signals. The latter task of signal processing was the most critical for developing practical vibro-electromagnetic systems. The unwanted background signals could be due to reflections from the operator of the system or other people near the intended subject. Since the MW signals penetrate dielectric materials, there may also be unwanted time-varying reflections from the movement of foliage, animals, traffic, or other nearby physical movements. This required creation of antennae with minimal side and back lobes in directional sensitivity pattern, or development of algorithms to suppress reflections from those zones.

The main applications of vibro-electromagnetic sounding could be:

- Detection of living persons under rubble or snow after some natural or technological disaster. The task made urgent by need for rescuers to focus their efforts on places where there is hope for retrieving living persons.
- Detection of people and parameters related to their physical and mental state at antiterrorist operations of law enforcement.
- Remote diagnostics of the psychological state of persons during covert or open screening; for example at airport security checkpoints.
- Contactless measurement of pulse and respiration for patients for whom contact sensors might be contra-indicated (e.g. burn patients or those with sleep disorders).

Further advances in sensitivity and signal processing, with machine learning, could even lead to recognition of speech using vibro-electromagnetic rather than acoustic recording.

Traditionally, for such biomedical applications, impulse radars operating in the waveband 3 cm to 30 cm were used [125], [127], [128]. However, HSR could also be useful for these applications as proposed in [124]. In this study, through-wall sounding was demonstrated using CW signals modulated by human heartbeat and breathing. A modified RASCAN HSR was used, having the following characteristics:

- Operating frequency: 1.6 GHz (λ =19 cm in air)
- Gain factor: 40 dB
- Frequency range of modulated recorded signals: 0.03 Hz to 3.0 Hz
- Dynamic range: 60 dB
- Sampling frequency: 20 Hz
- Antenna aperture: 120 mm

Preprints (www.preprints.org) | NOT PEER-REVIEWED | Posted: 2 June 2021 doi:10.20944/preprints202106.0059.v1

- Antenna height: 200 mm.

A sketch of the experiment is shown below in Fig. 47. The human subject stood 1 m behind a 10-cm thick wall. The radar antenna was fastened directly on surface of wall. To decrease interference from back lobe reflections, the antenna and surrounding wall were veiled by radar-reducing fabric with dimensions of 2 m by 2 m. The reflected radar signals returning through the block were amplified and recorded in a computer.

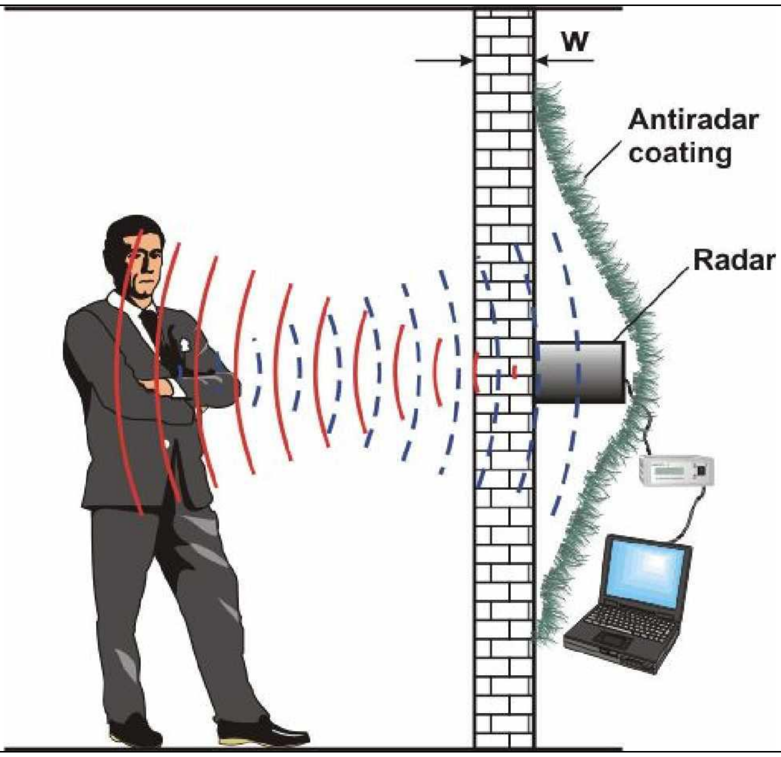

Fig. 47. Sketch of the experiment in [124]. Wall thickness W=10 cm

Figs. 48 and 49 present pulse records and their spectrums for the examinee after breath holds of various lengths. In Fig. 47, the breath hold was approximately 30 s, and in Fig. 48, the hold was about one minute. For the longer hold, the amplitude and rate of the subject's pulse increase due to oxygen starvation.

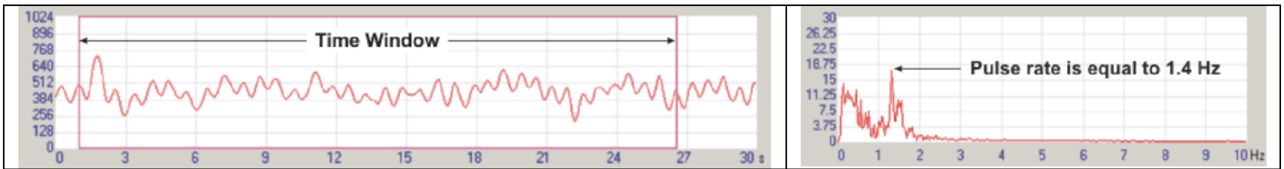

a) b)

Fig. 48. Pulse record of the examinee: a) signal and b) spectrum for a breath-hold of approximately 30 s.

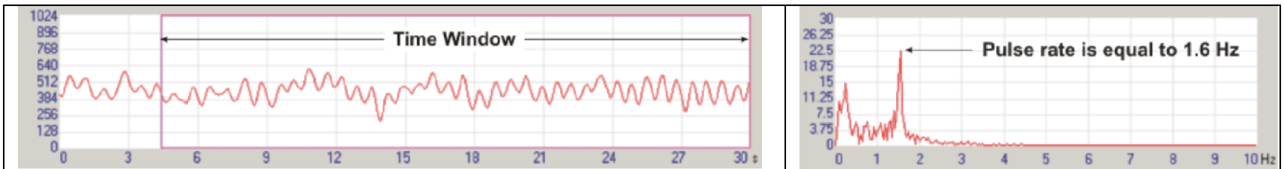

a) b)

Fig. 49. Pulse record of the examinee: a) signal and b) spectrum for a breath-hold of approximately 1 min.

The results of simultaneous recording of the pulse and breath rate of the subject are presented in Fig. 50. As the amplitude of oscillations and lung volume are considerably larger than for the heart, the movements of the cardiac muscle are observed as small high-frequency modulation on the background of larger lung/chest oscillations.

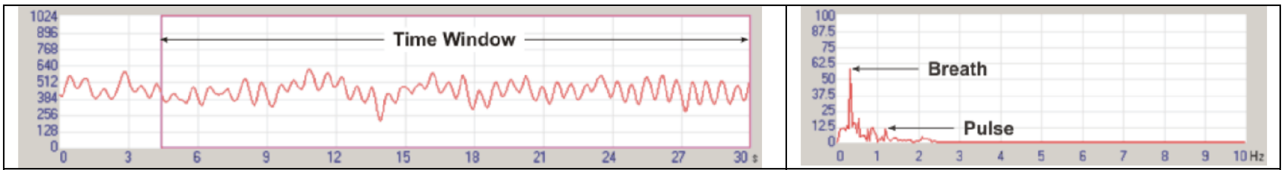

a) b)

Fig. 50. Breath and pulse record with no breath-hold; a) signal and b) spectrum.

A recording of speech is shown in Fig. 51. The subject repeated at a constant pace (in Russian) the words "one, two, three, one, two, three…". In this experiment, three processes were combined: heartbeat, breathing and articulation using the lips, throat and tongue. Considering that these processes are more difficult to separate in a vibro-electromagnetic record than in an acoustic recording, additional studies are needed to assess the possibility of isolating the speech component in the recorded MW. While the speech signal is clearly there, it is not yet possible to isolate or understand it.

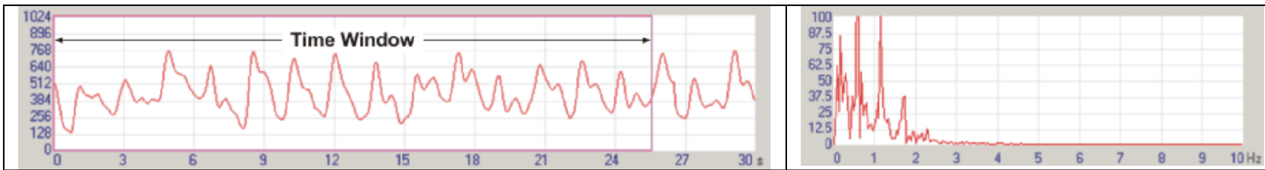

a) b)

Fig. 51. Breath and pulse record while the subject consistently repeats "one, two, three..." (in Russian); a) signal and b) spectrum.

The results obtained in the experiments in [124] are in many respects similar to the signals registered by time-domain impulse radars in free space [125]. However, use of monochromatic CW radar simplifies the experimental installation and subsequent data processing. These experiments on radar sounding of human pulse and breathing through a barrier (wall separating two adjacent rooms) demonstrate the technical feasibility of remote monitoring and diagnostics of humans using CW radars of RASCAN type.

The theoretical basis for signal processing of multi-frequency radar for detection of human breathing and heartbeat was discussed in [129]. The study assesses cross-correlation functions of different kinds applied to multi-frequency probing signals and determines the optimum processing sequence considering resolution, amplitudes of lateral lobes and the presence of diffractive maxima. The study models multi-frequency radar signals and their spectra modulated by breath and pulse for different distances or ranges. This analysis not only allows determination of the subject range, but facilitates rejection of signals from motionless or inactive nearby objects.

Other biomedical applications of HSR technology are related to more traditional medical imaging [56], [130], [131]. These applications primarily include breast cancer detection of the women [49], [132], [133], [134] and stroke features in the brain [135]. The potential advantage of MW technologies for the diagnosis of stroke is that the traditional computer aided tomography devices are good for diagnosing stroke, but they are expensive and very large devices. They can only be used in stationary installation such as hospitals. At the same time, prompt diagnosis (perhaps even in an ambulance) using a MW device could guide urgent measures to mitigate the effects of a stroke.

Preprints (www.preprints.org) | NOT PEER-REVIEWED | Posted: 2 June 2021 doi:10.20944/preprints202106.0059.v1

Breast cancer is common disease among women today. As a rule, traditional diagnostic procedures cannot guarantee identification of tumors. Since some may be aggressive or swiftly developing, there is a need for new methods which could detect the tumors at the earliest stage possible and/or be safely and easily repeated at close intervals. This problem may be solved with the help of HSR which detects dielectric inhomogeneities related to tumors. It is known that the dielectric properties of normal and malignant breast tissues differ even at the earliest stage of a tumor genesis. Thus, frequent scans with HSR could be used for safe early-stage breast tumor detection. In [133], a specially constructed model breast with two dielectrically realistic inclusions of various sizes simulating neoplasm was scanned using HSR at different frequencies. There was found that 4 GHz was preferable for breast inhomogeneity detection.

Among other applications of MW, it is also worth mentioning a proposal to use radar to monitor the living areas for old people to detect falls [57].

Although the undoubted advantage of MW methods is their almost complete safety compared to (for example) X-rays, the main obstacle is the high electrical conductivity of blood and other bodily fluids, which leads to a high level of attenuation of electromagnetic waves in the human body. For basic medical applications, a resolution of a few millimeters is required, which forces the use of sufficiently high frequencies. But with increasing frequency, the attenuation of electromagnetic waves also increases, which limits their penetration deep into the human body. Determining the compromise between attenuation and resolution requires additional research efforts.

4.5. Security

Modern security systems that use active MW technology generally record the complex amplitude of reflected waves from an area under surveillance and process these signals to produce images that may reveal concealed objects. These security systems are classified into two categories. The first includes mechanical scanning systems while the second includes electronic scanning systems [50]. For both categories, during scanning and data acquisition, the electromagnetic field is the same. For the second category, it can be estimated that electronic scanning can be completed in about ten times less time than systems with mechanical scanning [136]. The high acquisition rate in electronically scanned radar systems enables MW video streaming at frame rates of dozens per second. There are already several systems on the market and therefore a large-scale experimentation; among these are the ProVision [137] system produced by L-3 Communications which uses mechanical scanning by means of a series of vertically distributed elements, and the Eqo [138] radar system produced by Smiths Detection which uses the electronic control of a matrix 2 -D of distributed elements; through the electronic programming of the relative delays between the transmitting elements it is possible to define the point of focus within the investigable volume to provide a high resolution radar image [139]. The performance of the ProVision system, as mentioned in the data sheet [137], is between 200 and 300 people per hour at a data acquisition time of 1.5 seconds. The performance of Eqo should not exceed that of ProVision because it is based on the cooperative self-rotation of the investigated subject on a single point, which is difficult to obtain in less than 1.5 seconds. The performance of both systems is further limited by the fact that people often have to remove outer clothing before scanning. System performance limitations and high cost (approximately $ 170,000) limit use outside of airports, where security is needed for crowded public places. To increase the throughput of active radar systems while decreasing system cost, a system architecture based on the principle of inverse aperture synthesis has been proposed. This concept is different from the systems with mechanical scanning in that it uses the motion of subjects through an array of stationary transmitters to form a synthetic aperture. Systems that use such aperture synthesis are currently used in radar systems for tracking aerial or marine targets (planes and ships). In these systems, one of the difficulties arises from not knowing target parameters that would allow calculation of matched filter coefficients for signal processing. These

Preprints (www.preprints.org) | NOT PEER-REVIEWED | Posted: 2 June 2021 doi:10.20944/preprints202106.0059.v1

difficulties can be overcome when the target is a moving person by recording a synchronous video that captures the motion parameters of the walking subject as in Fig. 52 [52], [136]. These parameters will enable coherent radar processing and inverse aperture synthesis leading to a synthesized radar image, which can be calculated for every instantaneous pose of the walking person. A synthesized image can be calculated using the whole radar and video record acquired during the time that the subject occupies the surveillance area.

The proposed principle has been tested in laboratory conditions and shown to be practically applicable. Using an experimental setup with a mannequin subject (Fig. 53), it was shown that the proposed method can significantly reduce the dimensions of a prospective screening system and the number of channels in the antenna system and at the same time obtain detailed radar images of hidden objects.

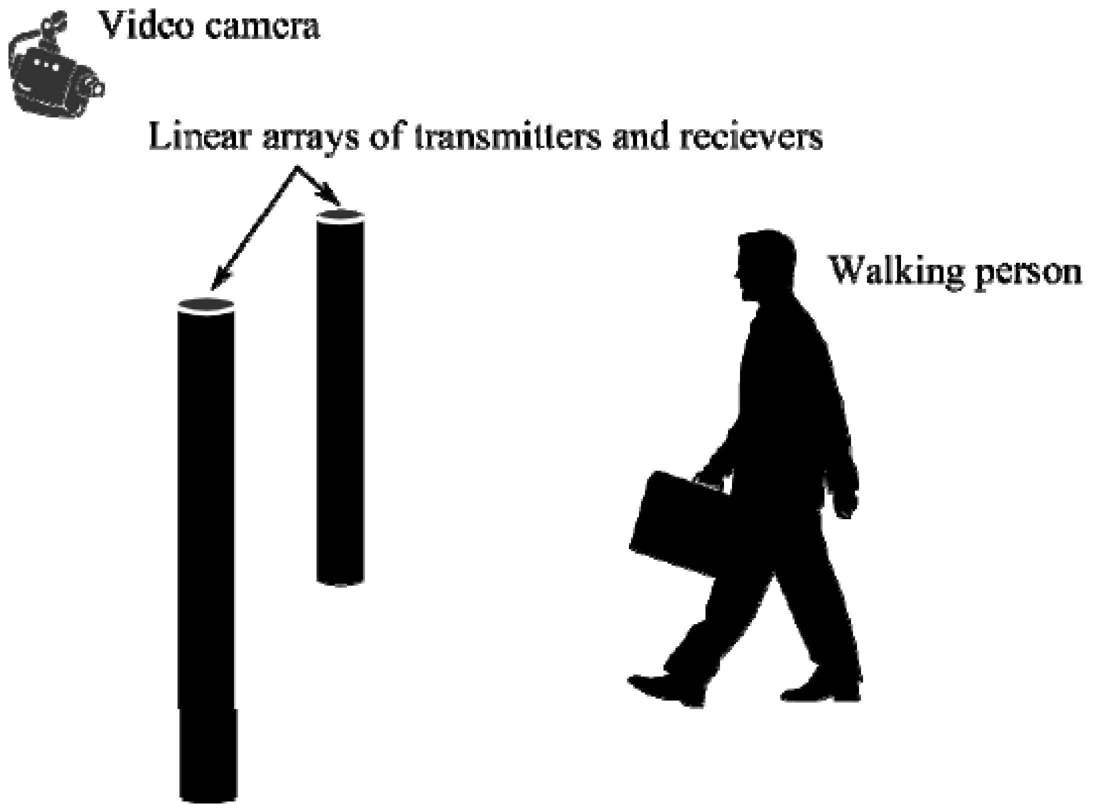

Fig. 52. The picture depicts the method of the radar system for inverse aperture synthesis including radar and a video camera.

The data obtained in an experiment with the mannequin are shown in Fig. 52 [51]. The data acquisition was done with the following parameters:

- the distance from the mannequin to the scan plane was about 45 cm
- the frequency of VNA sweeps was 18.0 GHz to 26.5 GHz
- the height and width of the scanned aperture were 100 cm and 90 cm, respectively.

In the reconstructed MW hologram (Fig. 53), the silhouette of the plastic mannequin is visible, as well as the metal belt buckle, and especially the highly reflective metal weapons. Further development of the proposed method and evaluation of its performance are underway using an electronically switched antenna array. This allows more rapid and representative data collection.

a)

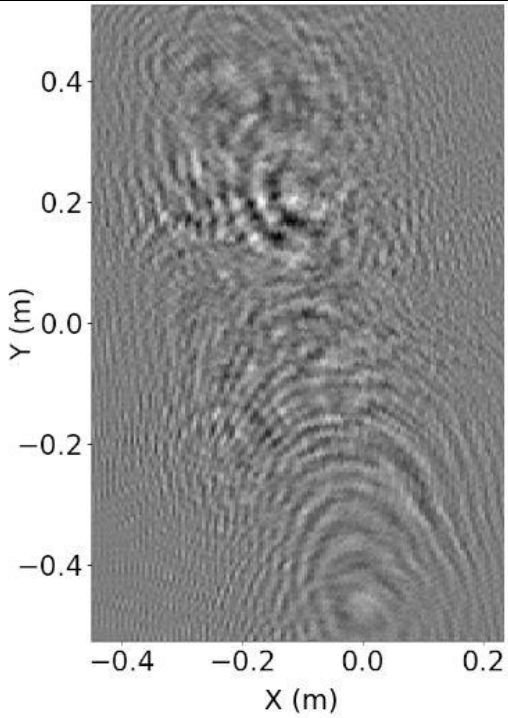

b)

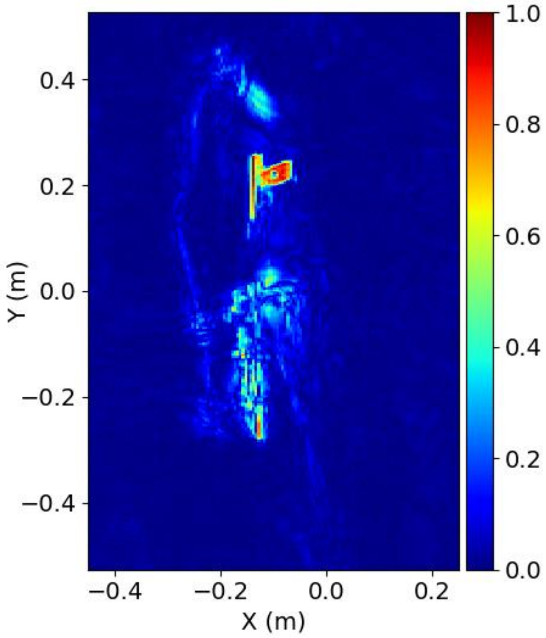

c)

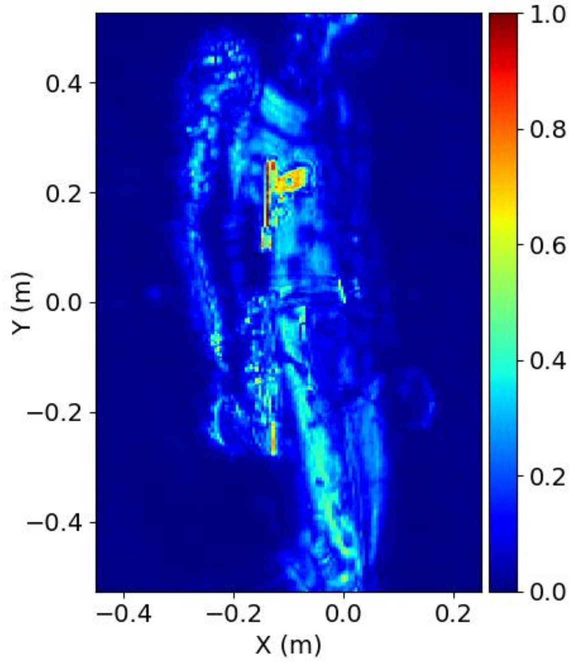

d)

Fig. 53. Experimental results:

a) Photograph of the mannequin with concealed objects: gun and knife
b) Real part of a fragment of the original hologram at the frequency of 22 GHz with the mannequin at the distance of around 45 cm from the scanned aperture
c) Radar image of the mannequin at the distance of 45 cm
d) Radar image of the mannequin obtained by a maximum projection.

VI. CONCLUSIONS

This review provides a summary of the theory, technology and applications of HSR including NDT, humanitarian demining, cultural heritage investigations, biomedical monitoring, and security. While HSR is not a universally applicable method for sounding of optically media, there are many (and growing) practical and important cases. With selection of appropriate probing signal frequency to balance the trade-off between scanning depth and plan-view resolution, it is possible to reconstruct microwave holograms of shallow targets that allow accurate determination of the shape and dimensions, and provide images suitable for human or machine classification. The case histories summarized here indicate promising prospects for even better subsurface imaging based on combining HSR with other sensors (e.g. optical, magnetic, acoustic) and with manual spatial sampling replaced by more precise robotic and/or electromechanical scanners.

ACKNOWLEDGEMENT

This review was prepared by international team of authors from Russia, USA, Italy, Bulgaria and Turkey, and supported by a few founds including the Russian Science Foundation under project # 21-19-00043, the Russian Foundation for Basic Research under projects #19-57-18001 and # 20-57-46004, and Bulgarian National Science Fund under administrative contract # KP-06-RUSSIA /22-28.09. 2019.

References

[1] M. I. Finkelstein, “Subsurface radar,” *Telecomm. Radio Eng.* Part 2, vol. 32, 1977, pp. 18-26 (English translation).

[2] D. J. Daniels, *Surface-penetrating radar*. Pub. by IEE. London, 1996.

[3] M.I. Finkelstein, V.A. Kutev, and V.P. Zolotarev, *Applications of subsurface radar in geology*, Nedra, Moscow, 1986 (in Russian).

[4] Doolittle, J.A., 1987. Using ground penetrating radar to increase the quality and efficiency of soil surveys. *Soil survey techniques*, *20*, pp.11-32.

[5] K. Iizuka, "Microwave hologram by photoengraving," in *Proceedings of the IEEE*, vol. 57, no. 5, pp. 813-814, May 1969, DOI: 10.1109/PROC.1969.7090.

[6] Iizuka, K. and Gregoris, L.G. (1970). Application of microwave holography in the study of the field from a radiating source. Appl. Phys. Lett. 17: 509–512.

[7] G. Junkin; and A. P. Anderson, “Limitations in microwave holographic synthetic aperture imaging over a lossy half-space,” *Communications, Radar and Signal Processing, IEE Proceedings F*, Volume 135, Issue 4, August 1988, pp. 321 – 329. DOI: 10.1049/ip-f-1.1988.0039

[8] Sergey I. Ivashov, Vladimir V. Razevig, Igor A. Vasiliev, Andrey V. Zhuravlev, Timothy D. Bechtel, and Lorenzo Capineri, Holographic Subsurface Radar of RASCAN Type: Development and Applications, IEEE Journal of Selected Topics in Earth Observations and Remote Sensing, Volume 4, Issue 4, December 2011. pp. 763-778. DOI: 10.1109/JSTARS.2011.2161755

[9] S.I. Ivashov, V.V. Razevig, A.P. Sheyko, I.A. Vasilyev, A Review of the Remote Sensing Laboratory's Techniques for Humanitarian Demining, Proceedings of International Conference on Requirements and Technologies for the Detection, Removal and Neutralization of Landmines and UXO, EUDEM2-SCOT-2003, 15-18 September 2003, Vrije Universiteit Brussel, Brussels, Belgium, 2003, Vol. 1, pp 3-8.

[10] X. J. Song, Y. Su, C. L. Huang, M. Lu, S. P. Zhu, “Landmine Detection with Holographic Radar,” *16th International Conference of Ground Penetrating Radar* (GPR 2016), Hong Kong, 13–16 June 2016, pp. 1–4. DOI: 10.1109/ICGPR.2016.7572660
[11] G. Pochanin, L. Capineri, T. Bechtel, V. Ruban, P. Falorni, F. Crawford, T. Ogurtsova, L. Bossi, "Radar Systems for Landmine Detection: Invited Paper," *2020 IEEE Ukrainian Microwave Week (UkrMW)*, Kharkiv, Ukraine, 2020, pp. 1118-1122, doi: 10.1109/UkrMW49653.2020.9252789
[12] D. Gabor, “A new microscopic principle,” *Nature*, 161, 1948, pp. 777-778, DOI: 10.1038/161777a0
[13] N. P. Chubinsky, “Possibilities of holographic methods at sounding of lossy media”, *Proceedings of 4th Russian conference Radio-Physics Methods in Remote Sensing*, Murom, 30 June – 3 July 2009, pp. 47-60 (in Russian).
[14] R.J. Collier, C.B Burckhardt, L.H. Lin, *Optical Holography*, Academic Press, New York and London, 1971.
[15] Wood, Robert Williams, *Physical Optics*, New York: The MacMillan Company, 1911, pp. 37–39.
[16] E.N. Leith, and J. Upatnieks, “Reconstructed wave fronts and communication theory,” J. Opt. Soc. America, 52, No. 4. XIV Advertisement, 1962, Available: http://www.opticsinfobase.org/viewmedia.cfm?uri=josa-52-10-1123&seq=0 .
[17] D. L. McMakin, D .M. Sheen, J. W. Griffin, and W. M. Lechelt. “Extremely high-frequency holographic radar imaging of personnel and mail,” Sensors, and Command, Control, Communications, and Intelligence (C31) Technologies for Homeland Security and Homeland Defense V, edited by Edward M. Carapezza, Proc. of SPIE Vol. 6201, 62011W, 2006. DOI: 10.1117/12.668509
[18] Andrey Zhuravlev, Vladimir Razevig, Margarita Chizh, and Sergey Ivashov, Imaging of concealed objects on moving persons by creating synthetic aperture due to their natural motion, Proceedings of the IEEE International Conference on Microwaves, Communications, Antennas and Electronic Systems (COMCAS 2017), Tel-Aviv, Israel, 13-15 November 2017, Pages: 1–4, DOI: 10.1109/COMCAS.2017.8244743
[19] V.V. Razevig, S.I. Ivashov, I.A. Vasiliev, A.V. Zhuravlev, T. Bechtel, L. Capineri, Advantages and Restrictions of Holographic Subsurface Radars. Experimental evaluation, Proceedings of the XIII International Conference on Ground Penetrating Radar, Lecce, Italy, 21-25 June 2010, pp. 657-662. DOI:10.1109/ICGPR.2010.5550241
[20] V. Razevig, S. Ivashov, M. Chizh, A. Zhuravlev and L. Capineri, "Influence of Electrical Properties of Media on Reconstruction of Microwave Holograms Recorded by Subsurface Radar," 2019 IEEE International Conference on Microwaves, Antennas, Communications and Electronic Systems (COMCAS), Tel-Aviv, Israel, 2019, pp. 1-5. DOI: 10.1109/COMCAS44984.2019.8958377
[21] V. Razevig, S. Ivashov, I. Vasiliev, A. Zhuravlev, Comparison of Different Methods for Reconstruction of Microwave Holograms Recorded by the Subsurface Radar, Proceeding of the 14th International Conference on Ground Penetrating Radar, 4-8 June 2012, Shanghai, China, pp. 335-339. DOI: 10.1109/ICGPR.2012.6254884
[22] Kolandasami A.P., Makhmanazarov R.M., Kuz`menko I.Y., Muksunov T.R., Yakubov V.P. Phase as the basis for wave vision //IOP Conf. Ser.: Mater. Sci. Eng. 2019. Vol. 516. P. 1-5. URL: https://iopscience.iop.org/article/10.1088/1757-899X/516/1/012058
[23] http://www.rslab.ru/downloads/scan.avi
[24] E. Bechtel, S. Ivashov, T. Bechtel, E. Arsenyeva, A. Zhuravlev, I. Vasiliev, V. Razevig, and A. Sheyko, “Experimental determination of the resolution of the RASCAN-4/4000 holographic radar system,” 12th International Conference on Ground Penetrating Radar, June 16-19, 2008, Birmingham, UK. http://www.rslab.ru/downloads/bechtel_et_al.pdf

[25] C. Liu, M. T. Al Qaseer and R. Zoughi, "Influence of Antenna Pattern on Synthetic Aperture Radar Resolution for NDE Applications," in *IEEE Transactions on Instrumentation and Measurement*, DOI: 10.1109/TIM.2020.3026122.

[26] T. Lu, C. Snapp, T.-H. Chao, A. Thakoor, T. Bechtel, S. Ivashov, I. Vasiliev, "Evaluation of holographic subsurface radar for NDE of space shuttle thermal protection tiles," *Sensors and Systems for Space Applications. Proceedings of SPIE*, Volume 6555, 2007. DOI: 10.1117/12.719911

[27] S. I. Ivashov, V. V. Razevig, A. V. Zhuravlev, T. Bechtel and M. A. Chizh, "Comparison of Different NDT Methods in Diagnostics of Rocket Cryogenic Tanks Thermal Protection Coating," 2019 IEEE International Conference on Microwaves, Antennas, Communications and Electronic Systems (COMCAS), Tel-Aviv, Israel, 2019, pp. 1-5. DOI: 10.1109/COMCAS44984.2019.89581577

[28] S. Kharkovsky and R. Zoughi, "Microwave and millimeter wave nondestructive testing and evaluation," *IEEE Instrum. Meas. Mag.*, April 2007, 10(2), pp. 26–38. DOI: 10.1109/MIM.2007.364985

[29] J. T. Case, F.L. Hepburn, R. Zoughi, Inspection of Spray on Foam Insulation (SOFI) Using Microwave and Millimeter Wave Synthetic Aperture Focusing and Holography, 2006 IEEE Instrumentation and Measurement Technology Conference Proceedings, Sorrento, Italy, 24-27 April 2006. DOI: 10.1109/IMTC.2006.328527

[30] L. Capineri, P. Falorni , T. Becthel, S. Ivashov , V. Razevig and A. Zhuravlev, Water detection in thermal insulating materials by high resolution imaging with holographic radar, Measurement Science and Technology, Special Issue, Vol. 28, No. 1, 2017, pp. 1-6. DOI:10.1088/1361-6501/28/1/014008

[31] X. Zhang, J. Liang, N. Wang, T. Chang, Q. Guo and H. Cui, "Broadband Millimeter-Wave Imaging Radar-Based 3-D Holographic Reconstruction for Nondestructive Testing," in *IEEE Transactions on Microwave Theory and Techniques*, vol. 68, no. 3, pp. 1074-1085, March 2020, DOI: 10.1109/TMTT.2019.2948349.

[32] R. K. Amineh, M. Ravan and R. Sharma, "Nondestructive Testing of Nonmetallic Pipes Using Wideband Microwave Measurements," in *IEEE Transactions on Microwave Theory and Techniques*, vol. 68, no. 5, pp. 1763-1772, May 2020, DOI: 10.1109/TMTT.2020.2969382.

[33] Chao Liu, Al Qaseer Mohammad Tayeb, Forrest Sheng Bao, Reza Zoughi, Target depth-based adaptive scanning in microwave synthetic aperture radar imaging for NDE applications, Proceedings SPIE, Volume 11745, Passive and Active Millimeter-Wave Imaging XXIV; 1174509 (2021), https://doi.org/10.1117/12.2585930.

[34] Andreas Och , Patrick A. Hölzl, Stefan Schuster, Stefan Scheiblhofer, Dominik Zankl, Venkata Pathuri-Bhuvana, and Robert Weigel, "High-Resolution Millimeter-Wave Tomography System for Nondestructive Testing of Low-Permittivity Materials," in IEEE Transactions on Microwave Theory and Techniques, vol. 69, no. 1, pp. 1105-1113, Jan. 2021, doi: 10.1109/TMTT.2020.3030662

[35] S. I. Ivashov, V. I. Makarenkov, V. V. Razevig, V. N. Sablin, A. P. Sheyko, I. A. Vasiliev, "Concrete floor inspection with help of subsurface radar," *Eight International Conference on Ground-Penetrating Radar*, GPR'2000, May 23-26, 2000, University of Queensland, Gold Coast, Queensland, Australia, pp. 552-555. DOI: 10.1117/12.383629.

[36] L. Capineri, P. Falorni, G. Borgioli, A. Bulletti, S. Valentini, S. Ivashov, A. Zhuravlev, V. Razevig, I. Vasiliev, M. Paradiso, M. Inagaki, C. Windsor, T. Bechtel, "Application of the RASCAN holographic radar to cultural heritage inspections," Archaeological Prospection, 16, pp. 218-230, 2009. DOI: 10.1002/arp.360

[37] V. V. Razevig, S. I. Ivashov, A. P. Sheyko, I. A. Vasilyev and A. V. Zhuravlev, An example of holographic radar using at restoration works of historical building, Progress In Electromagnetics Research Letters, Vol. 1, pp. 173–179, 2008. DOI: 10.2528/PIERL07120603

[38] Sergey Ivashov, Timothy Bechtel, Vladimir Razevig, Lorenzo Capineri, and Masaharu Inagaki, A proposed radar method for non-destructive investigation of Egyptian pyramids, Insight, January 2021, Vol 63, No 1, pp. 12-19. DOI: DOI: 10.1784/insi.2021.63.1.12.
[39] Vasiliev I.A., Ivashov S.I., Makarenkov V.I., Sablin V.N., Sheyko A.P. RF Band High Resolution Sounding of Building Structures and Works. IEEE Aerospace & Electronic Systems Magazine. May 1999, Vol. 14, No. 5, pp. 25-28. DOI: 10.1109/62.765776
[40] Luca Bossi, Pierluigi Falorni, Colin Windsor, Fabiana Zandonai, Fabrizio Bizzarini, Massimo Delfino, Luca Giusberti, Timothy Bechtel, Margarita Chizh, Sergey Ivashov, Lorenzo Capineri, The imaging of subsurface crocodile remains in a limestone slab using holographic radar, GPR 2020 — 18th International Conference on Ground Penetrating Radar, Golden, Colorado USA, June 14–19, 2020, pp. 6-9. DOI: 10.1190/gpr2020-003.1
[41] S. Ivashov, V. Razevig, A. Zhuravlev, M. Chizh, T. Bechtel, L. Capineri, M. Inagaki, MW Holographic Imaging System for Detection of Hidden Dinosaur Tracks, The 38th PIERS in St Petersburg, Russia, 22 - 25 May, 2017, Pages: 3241-3246, DOI: 10.1109/PIERS.2017.8262316
[42] Vohra, D., Bechtel, T., Thomas, R.D.K., Windsor, C., Ivashov, S., Capineri, L., Inagaki, M. and Van Scyoc, R., 2015, July. A test of holographic radar for detection of hidden vertebrate tracks and trackways. In 2015 8th International Workshop on Advanced Ground Penetrating Radar (IWAGPR) (pp. 1-4). IEEE
[43] T. Bechtel, L. Capineri, C. Windsor, M. Inagaki, S. Ivashov, Comparison of ROC curves for landmine detection by holographic radar with ROC data from other methods, 2015 8th International Workshop on Advanced Ground Penetrating Radar (IWAGPR), 2015, p. 1-4, DOI: 10.1109/IWAGPR.2015.7292645
[44] G. Borgioli, L. Bossi, L. Capineri, P. Falorni, T. Bechtel, F. Crawford, M. Inagaki, G. Pochanin, V. Ruban, L. Varyanitza-Roschupkina, and T. Ogurtsova, "A Hologram Reconstruction Algorithm for Landmine Recognition and Classification Based on Microwave Holographic Radar Data," *2018 Progress in Electromagnetics Research Symposium (PIERS-Toyama)*, Toyama, 2018, pp. 1938-1944, doi: 10.23919/PIERS.2018.8597707.
[45] S.I. Ivashov, V.N. Sablin and I.A. Vasilyev, "Wide-span systems of mine detection," in *IEEE Aerospace and Electronic Systems Magazine*, vol. 14, no. 5, pp. 6-8, May 1999, DOI: 10.1109/62.765772.
[46] S. I. Ivashov, V. N. Sablin, I. A. Vasilyev, N. V. Nikiforov and V. E. Minkov, "Wide-span systems of mine detection," 1998 Second International Conference on the Detection of Abandoned Land Mines (IEE Conf. Publ. No. 458), Edinburgh, UK, 1998, pp. 78-80, DOI: 10.1049/cp:19980693.
[47] A. Zhuravlev, A. Bugaev, S. Ivashov, V. Razevig and I. Vasiliev, "Microwave holography in detection of hidden objects under the surface and beneath clothes," 2011 XXXth URSI General Assembly and Scientific Symposium, Istanbul, 2011, pp. 1-4, DOI: 10.1109/URSIGASS.2011.6050429
[48] A. Zhuravlev, V. Razevig, M. Chizh, and S. Ivashov, Imaging of concealed objects on moving persons by creating synthetic aperture due to their natural motion, Proceedings of the IEEE International Conference on Microwaves, Communications, Antennas and Electronic Systems (COMCAS 2017), Tel-Aviv, Israel, 13-15 November 2017, pp. 1–4, DOI: 10.1109/COMCAS.2017.8244743
[49] Meng, Y.; Lin, C.; Zang, J.; Qing, A.; Nikolova, N.K. Ka Band Holographic Imaging System Based on Linear Frequency Modulation Radar. *Sensors* **2020**, *20*, 6527. DOI: 10.3390/s20226527
[50] Sheen D.M., McMakin D.L., Hall T.E., Three-dimensional millimeter-wave imaging for concealed weapon detection, IEEE Trans. Microwave Theory Tech., vol. 49, no. 9, pp. 1581–1592, Sep. 2001. DOI: 10.1109/22.942570

[51] Zhuravlev, A., Razevig, V., Chizh, M., Dong, G., Hu, B. (2020). A New Method for Obtaining Radar Images of Concealed Objects in Microwave Personnel Screening Systems. IEEE Transactions on Microwave Theory and Techniques, *1–1*. DOI:10.1109/tmtt.2020.3023443

[52] David M. Sheen, R. Trevor Clark, J. Tedeschi, A. Mark Jones, Thomas E. Hall, "High-resolution 3D microwave imaging of a moving target using optical motion capture," Proc. SPIE 10994, Passive and Active Millimeter-Wave Imaging XXII, 109940D (13 May 2019); doi: 10.1117/12.2519892

[53] J. Gao, Y. Qin, B. Deng, H. Wang and X. Li, "A Novel Method for 3-D Millimeter-Wave Holographic Reconstruction Based on Frequency Interferometry Techniques," in IEEE Transactions on Microwave Theory and Techniques, vol. 66, no. 3, pp. 1579-1596, March 2018, doi: 10.1109/TMTT.2017.2772862.

[54] Bechtel, T., Capineri, L., Falorni, P., Inagaki, M., Zhuravlev, A., Razevig, V., Ivashov, S. and Windsor, C., 2011, March. Detection of Latent Damage from Insect Activity in Wooden Structures through the Use of Holographic Subsurface Radar. In *PIERS Proceedings*, Marrakesh, Morocco, March 2011, p. 95.

[55] L. N. Anishchenko, I. L. Alborova, M. A. Chizh and A. V. Zhuravlev, "Microwave imaging of biological tissue phantom in different frequency ranges," *2016 Progress in Electromagnetic Research Symposium (PIERS)*, Shanghai, 2016, pp. 4639-4643, doi: 10.1109/PIERS.2016.7735712

[56] C. Huang, T. Liu, M. Lu and Y. Su, "Holographic subsurface imaging for medical detection," *Proceedings of the 15th International Conference on Ground Penetrating Radar*, Brussels, 2014, pp. 651-654, DOI: 10.1109/ICGPR.2014.6970506.

[57] Anishchenko, L., Zhuravlev, A., & Chizh, M. (2019). Fall Detection Using Multiple Bioradars and Convolutional Neural Networks. Sensors, 19(24), 5569. DOI: 10.3390/s19245569

[58] D. Flores-Tapia, O. Maizlish, C. M. Alabaster and S. Pistorius, "A holographic reconstruction method for circular multistatic subsurface radar," *2012 International Waveform Diversity & Design Conference (WDD)*, Kauai, HI, 2012, pp. 142-145, DOI: 10.1109/WDD.2012.7311268.

[59] H. Wu, M. Ravan and R. K. Amineh, "Holographic Near-Field Microwave Imaging With Antenna Arrays in a Cylindrical Setup," in *IEEE Transactions on Microwave Theory and Techniques*, DOI: 10.1109/TMTT.2020.3031897.

[60] I.A. Vasiliev, A.I. Ivashov, S.I. Ivashov, V.I. Makarenkov, V.N. Sablin, A.P. Sheiko, Subsurface radar, Russian patent # 2158015, 20.10.2000, RU 2 158 015 C2. Reference in WoS: http://apps.webofknowledge.com/full_record.do?colName=DIIDW&recordID=2001101210&log_event=no&search_mode=GeneralSearch&qid=2&log_event=yes&product=UA&SID=C6FUAJCOAHXc12dYwqC&viewType=fullRecord&doc=3&page=1

[61] Luca Bossi, Pierluigi Falorni, Alessandro Bartolini, Lorenzo Capineri, Characterization of a 2 GHz holographic radar antenna for detection of subsurface targets, 18th International Conference on Ground Penetrating Radar, Golden, Colorado, 14–19 June 2020, pp. 324-327. DOI: 10.1190/gpr2020-085.1

[62] S.I. Ivashov, L. Capineri, and T.D. Bechtel, Holographic Subsurface Radar Technology and Applications, in book UWB Radar. Applications and Design, edited by James J. Taylor, CRC Press, Taylor & Francis Group, 2012, pp. 421-444. ISBN 978-1-4200-8986-8.

[63] http://www.rslab.ru/downloads/ptm3.avi

[64] V.V. Razevig, I.A. Vasil'ev, A.I. Ivashov, S.I. Ivashov, V.I. Makarenkov, Method of Obtaining Radio Holograms of Subsurface Objects, Russian patent #2482518, 01.11.2011. http://apps.webofknowledge.com/full_record.do?colName=DIIDW&recordID=2013H61403&log_event=no&search_mode=GeneralSearch&qid=9&log_event=yes&product=UA&SID=F1YM3JgCMcXP2VTvp7o&viewType=fullRecord&doc=2&page=1

[65] http://www.rslab.ru/english/product

[66] Andrey Zhuravlev, Sergey Ivashov, Igor Vasiliev, Vladimir Razevig, Processing of Holographic Subsurface Radar Data, Proceeding of the 14th International Conference on Ground Penetrating Radar. 4-8 June 2012, Shanghai, China, pp. 68-71. DOI:10.1109/icgpr.2012.6254833

[67] S. Ivashov, V. Razevig, I. Vasiliev, T. Bechtel, L. Capineri, Holographic subsurface radar for diagnostics of cryogenic fuel tank thermal insulation of space vehicles, NDT & E International, Vol. 69, January 2015, Pages 48-54, DOI: 10.1016/j.ndteint.2014.10.002

[68] A. V. Zhuravlev, S. I. Ivashov, V. V. Razevig, I. A. Vasiliev and A. S. Bugaev, "Holographic subsurface radar RASCAN-5," 2013 7th International Workshop on Advanced Ground Penetrating Radar, Nantes, 2013, pp. 1-6. DOI: 10.1109/IWAGPR.2013.6601548

[69] J.V. Goodman, Introduction to Fourier Optics. New York: McGraw-Hill, 2005.

[70] Tikhonov A. N. Solutions of Ill-Posed Problems, New York, Winston, 1977.

[71] A. V. Popov, V. V. Kopeikyn, V. A. Vinogradov and S. A. Zapunidi, "Reconstruction algorithms and experiments with a prototype of holographic subsurface radar," *4th International Conference on Antenna Theory and Techniques (Cat. No.03EX699)*, Sevastopol, Ukraine, 2003, pp. 561-563 vol.2, doi: 10.1109/ICATT.2003.1238803.

[72] A. Popov, I. Prokopovich and D. Edemskii, "Experimental implementation of microwave subsurface holography," *2016 Days on Diffraction (DD)*, St. Petersburg, 2016, pp. 340-345, DOI: 10.1109/DD.2016.7756870

[73] Y. Zhang, Z. Xiao, L. Wu, X. Lu and Y. Wang, "Deep learning for subsurface penetrating super-resolution imaging," *2017 10th UK-Europe-China Workshop on Millimetre Waves and Terahertz Technologies (UCMMT)*, Liverpool, 2017, pp. 1-4, DOI: 10.1109/UCMMT.2017.8068492.

[74] D. Sukhanov and K. Zavyalova, "Three-dimensional non-contact subsurface radiotomography through a non-planar interface between media," *Proceedings of the 15th International Conference on Ground Penetrating Radar*, Brussels, 2014, pp. 663-667, DOI: 10.1109/ICGPR.2014.6970509

[75] V.V. Razevig, A.V. Zhuravlev, A.S. Bugaev, M.A. Chizh and S.I. Ivashov, "Imaging under irregular surface using microwave holography," 2017 Progress in Electromagnetics Research Symposium - Fall (PIERS - FALL), Singapore, 2017, pp. 172-177. DOI: 10.1109/PIERS-FALL.2017.8293132

[76] Qin, T., Bossi, L., Bartolini, A., Falorni, P., Giannelli, P., Zhao, Y., & Capineri, L. (2018). *Influence Analysis of Uneven Surface on Landmine Detection Using Holographic Radar. 2018 Progress in Electromagnetics Research Symposium (PIERS-Toyama).* doi:10.23919/piers.2018.8597927

[77] https://www.geophysical.com/about-gssi

[78] https://www.guidelinegeo.com/

[79] Ivashov S.I., Makarenkov V.I., Razevig V.V., Sablin V.N., Sheyko A.P., Vasiliev I.A. Remote Control Mine Detection System with GPR and Metal Detector. Eight International Conference on Ground-Penetrating Radar, GPR'2000, May 23-26, 2000, University of Queensland, Gold Coast, Queensland, Australia, pp. 36-39. DOI: 10.1117/12.383598

[80] Reza K. Amineh, Natalia K. Nikolova, Maryam Ravan, Real Time Three Dimensional Imaging of Dielectric Bodies Using Microwave/Millimeter Wave Holography, Publisher: IEEE Press Series on RF and Microwave Technology, IEEE press, Wiley, June 2019, ISBN: 978-1-119-53886-8. DOI: 10.1002/9781119538875

[81] Landmine Monitor 2020, 12 Nov 2020, the-monitor.org/en-gb/reports/2020/landmine-monitor-2020.aspx

[82] V.P. Joynt, “Mobile metal detection: a field perspective,” Proceedings of the Second International Conference on the Detection of Abandoned Land Mines, MD’98. Edinburgh, UK, 12-16 October 1998, pp. 14,15.

[83] M. Sato, "Dual Sensor ALIS for Humanitarian Demining and its Evaluation Test in Mine Fields in Croatia," IGARSS 2008 - 2008 IEEE International Geoscience and Remote Sensing Symposium, Boston, MA, 2008, pp. II-181-II-184, DOI: 10.1109/IGARSS.2008.4778957.javascript:void(0)

[84] Jane's Mines and Mine Clearance Edition by Colin King, December 1, 1996.

[85] David Daniels; Jurgen Braunstein; and Michael Nevard, (2014) "Using MINEHOUND in Cambodia and Afghanistan," The Journal of ERW and Mine Action: Vol. 18: Issue 2, Article 14.

[86] S. Ivashov, V. Razevig, I. Vasilyev, A. Zhuravlev, T. Bechtel, L. Capineri, The Holographic Principle in Subsurface Radar Technology, International Symposium to Commemorate the 60th Anniversary of the Invention of Holography, Springfield, Massachusetts USA, October 27-29, 2008, pp. 183-197.

[87] Windsor, C., Capineri, L., & Bechtel, T. D. (2012). Buried object classification using holographic radar. Insight-Non-Destructive Testing and Condition Monitoring, 54(6), 331-339.

[88] T. Bechtel, G. Pochanin, S. Truskavetsky, M. Dimitri, V. Ruban, O. Orlenko, T. Byndych, A. Sherstyuk, K. Viatkin, F. Crawford, P. Falorni, A. Bulletti, L. Capineri, "Terrain Analysis in Eastern Ukraine and the Design of a Robotic Platform Carrying GPR Sensors for Landmine Detection," 2018 17th International Conference on Ground Penetrating Radar (GPR), Rapperswil, 2018, pp. 1-4, doi: 10.1109/ICGPR.2018.8441556.

[89] Capineri, L., Arezzini, I., Calzolai, M., Windsor, C., Inagaki, M., Bechtel, T., & Ivashov, S. (2013). High resolution imaging with a holographic radar mounted on a robotic scanner. Session 4A5 SC5: High Resolution Imaging with Penetrating Radar Scanners for Detection of Small or Low Contrast Objects, 1378.

[90] L Bossi, P Falorni, G Pochanin, V Ruban, T Ogurtsova, F Crawford, T. Bechtel, L. Capineri, Detection of targets from radar tracks of the UWB-GPR" 1Tx+ 4Rx" on the mobile platform" 18th International Conference on Ground Penetrating Radar, June 14-19, 2020, 448-451. DOI: 10.1190/gpr2020-116.1

[91] Jonard, F., Weihermüller, L., Vereecken, H., & Lambot, S. (2012). *Accounting for soil surface roughness in the inversion of ultrawideband off-ground GPR signal for soil moisture retrieval. GEOPHYSICS, 77(1), H1–H7.* doi:10.1190/geo2011-0054.1

[92] V. V. Razevig, A. V. Zhuravlev, A. S. Bugaev, M. A. Chizh and S. I. Ivashov, "Imaging under irregular surface using microwave holography," 2017 Progress in Electromagnetics Research Symposium - Fall (PIERS - FALL), Singapore, 2017, pp. 172-177. DOI: 10.1109/PIERS-FALL.2017.8293132

[93] Vladimir Razevig, Andrey Zhuravlev, Margarita Chizh, Sergey Ivashov, Alexander Bugaev, Hand-held Radar with Video Positioning System for Microwave Imaging, The 38th PIERS in St Petersburg, Russia, 22 - 25 May, 2017, Pages: 3052-3055, DOI: 10.1109/PIERS.2017.8262279

[94] A. Zhuravlev, V. Razevig, S. Ivashov, A. Skrebkov, V. Alekseev, On the Use of Microwave Holography to Detect Surface Defects of Rails and Measure the Rail Profile, Sensors 2019, 19, 1376, pp. 1–11. DOI: 10.3390/s19061376

[95] R. Zoughi *et al.*, "Real-time and on-line near-field microwave inspection of surface defects in rolled steel," *Proceedings of 1997 Asia-Pacific Microwave Conference*, Hong Kong, 1997, pp. 1081-1084 vol.3, doi: 10.1109/APMC.1997.656406

[96] Y. Gao *et al.*, "Millimeter Wave Differential Probe System for Surface Crack Detection in Painted Aircraft Fuselage," *2019 IEEE International Instrumentation and Measurement Technology Conference (I2MTC)*, Auckland, New Zealand, 2019, pp. 1-6, doi: 10.1109/I2MTC.2019.8826970

[97] M.T. Ghasr, Y. LePape, D.B. Scott, and R. Zoughi, "Holographical Microwave Imaging of Corroded Steel Bars in Concrete," *American Concrete Institute (ACI) Materials Journal*, vol. 112, no. 1, pp. 115-124, January 2015. doi:10.14359/51686981.

[98] Ivashov S.I., Makarenkov V.I., Razevig V.V., Sablin V.N., Sheyko A.P., Vasiliev I.A. Concrete Floor Inspection with Help of Subsurface Radar. Eight International Conference on Ground-Penetrating Radar, GPR'2000, May 23-26, 2000, University of Queensland, Gold Coast, Queensland, Australia, pp. 552-555. DOI: 10.1117/12.383629

[99] S. Ivashov, V. Razevig, A. Sheyko, I. Vasilyev, T. Bechtel, Holographic Radar as a Tool for Non-Destructive Evaluation of Structural Materials, Proceedings of the 2005 SEM Annual Conference & Exposition on Experimental and Applied Mechanics, Portland, Oregon, USA, Tuesday, June 7 - Thursday, June 9, 2005.

[100] Columbia Accident Investigation Board Report (2003), NASA, August.

[101] Gofin MYa. Heat resisting and thermal protecting systems of reusable space ships. Moscow: Mir; 2003. p. 672 (in Russian).

[102] Aviation Week & Space Technology. April 7, 2003, p. 31.

[103] Aviation Week & Space Technology. February 17, 2003, p. 27, 28.

[104] Aviation Week & Space Technology. October 4, 2004, p. 58.

[105] Ivashov S.I., Vasiliev I.A., Bechtel T.D., Snapp C., Comparison between impulse and holographic subsurface radar for NDT of space vehicle structural materials, Progress in electromagnetics research symposium. 2007, Beijing, China, March 26–30, 2007, p. 1816–1819.

[106] Sergey I. Ivashov, Vladimir V. Razevig, Timothy D. Bechtel, Igor A. Vasiliev, Lorenzo Capineri, and Andrey V. Zhuravlev, Microwave Holography for NDT of Dielectric Structures, Proceedings of the IEEE International Conference on Microwaves, Communications, Antennas and Electronic Systems (COMCAS 2015), Tel-Aviv, Israel, 2-4 November 2015, 978-1-4799-7473-3/15/$31.00 ©2015 IEEE, DOI: 10.1109/COMCAS.2015.7360372

[107] Ivashov, S., Zhuravlev, A., Chizh, M., & Razevig, V. (2016). *High resolution MW holographic system for NDT of dielectric materials and details. 2016 16th International Conference on Ground Penetrating Radar (GPR).* DOI:10.1109/icgpr.2016.7572595

[108] Margarita A. Chizh, Andrey V. Zhuravlev, Vladimir V. Razevig, and Sergey I. Ivashov, Experimental Validation of Sparse Sensing Technique in Subsurface Microwave Holography, PIERS in Shanghai, 8 - 11 August, 2016, pp. 1734-1738. DOI: 10.1109/PIERS.2016.7734775

[109] Sergey Ivashov, Andrey Zhuravlev, Vladimir Razevig, Margarita Chizh, Timothy Bechtel, Lorenzo Capineri, Binu Thomas, "Frequency Influence in Microwave Subsurface Holography for Composite Materials Testing," Proceedings of the 17th International Conference on Ground Penetrating Radar, GPR 2018, Rapperswil, Switzerland, June 18–21, 2018, pp. 98-103. DOI: 10.1109/ICGPR.2018.8441592

[110] Ivashov, S. I., Bugaev, A. S., Zhuravlev, A. V., Razevig, V. V., Chizh, M. A., & Ivashov, A. I. (2018). *Holographic Subsurface Radar Technique for Nondestructive Testing of Dielectric Structures. Technical Physics, 63(2), 260–267.* doi:10.1134/s1063784218020184

[111] M. Chizh, A. Zhuravlev, V. Razevig and S. Ivashov, "Detection of Water Inclusions in Honeycomb Composite Products by a Holographic Radar," 2019 IEEE International Conference on Microwaves, Antennas, Communications and Electronic Systems (COMCAS), Tel-Aviv, Israel, 2019, pp. 1-5. DOI: 10.1109/COMCAS44984.2019.8958114

[112] Reza K. Amineh, Maryam Ravan, and Raveena Sharma, Nondestructive Testing of Nonmetallic Pipes Using Wideband Microwave Measurements, IEEE Transactions on Microwave Theory and Techniques, accepted for publishing, DOI: sci-hub.do/10.1109/tmtt.2020.2969382

[113] A. Mazzinghi, A. Freni, L. Capineri, A microwave non-destructive testing method for controlling polymeric coating of metal layers in industrial products, NDT and E International, Vol. 102, March 2019, pp. 207–217 DOI: 10.1016/j.ndteint.2018.12.003

[114] Ur Rahman, M. S., Haryono, A., & Abou-Khousa, M. A. (2020). *Microwave Non-destructive Evaluation of Glass Reinforced Epoxy and High Density Polyethylene Pipes. Journal of Nondestructive Evaluation, 39(1).* doi:10.1007/s10921-020-00669-2

[115] M. A. Abou‐Khousa, A. Ryley, S. Kharkovsky, R. Zoughi, D. Daniels, N. Kreitinger, and G. Steffes, Comparison of X-Ray, Millimeter Wave, Shearography and Through-Transmission Ultrasonic Methods for Inspection of Honeycomb Composites, AIP Conference Proceedings 894, 999 (2007); DOI: 10.1063/1.2718076

[116] L. Capineri, P. Falorni, S. Ivashov, A. Zhuravlev, I. Vasiliev, V. Razevig, T. Bechtel and G. Stankiewicz, Combined holographic subsurface radar and infrared thermography for diagnosis of the conditions of historical structures and artworks, Near Surface Geophysics, 2010, 8, pp. 355-364. **DOI:** 10.3997/1873-0604.2010005

[117] Chaban, A., Deiana, R., & Tornari, V. (2020). *Wall Mosaics: A Review of On-Site Non-Invasive Methods, Application Challenges and New Frontiers for Their Study and Preservation. Journal of Imaging, 6(10), 108.* DOI: 10.3390/jimaging6100108

[118] S. Ivashov, L. Capineri, T. Bechtel, V. Razevig, A. Zhuravlev, and P. Falorni, Use of holographic subsurface radar analysis in the preservation and restoration of cultural heritage objects, Surface Topography: Metrology and Properties, 2019, v. 7, No. 4, 045017, pp. 1-11. DOI: 10.1088/2051-672X/ab4fa2

[119] L. Capineri, F. Zandonai, M. Inagaki, V. Razevig, S. Ivashov, C. Windsor, and T. Bechtel, RASCAN holographic radar for detecting and characterizing dinosaur tracks, Proceedings of the 2013 7th International Workshop on Advanced Ground-Penetrating Radar, July 02-05, 2013, Nantes, France, pp. 71-76. DOI: 10.1109/IWAGPR.2013.6601553

[120] Inagaki, M., Bechtel, T., Capineri, L., Ivashov, S., Windsor, C., A small difference of permittivity observed in a holographic radar image of dinosaur footprints, Conference: Society of Exploration Geophysics Japan, Tokyo, Lapan, Volume: 128th Conference, Spring 2013, June 2013, pp. 117-120, in Japanes. https://jglobal.jst.go.jp/detail?JGLOBAL_ID=201302261927363642

[121] Galton, P. M. and J. O. Farlow, "Dinosaur State Park, Connecticut, USA: History, footprints, trackways exhibits," *Zubia*, Nr. 21, 129–174, 2003.

[122] Kunihiro Morishima, Mitsuaki Kuno, Akira Nishio et al., Discovery of a big void in Khufu's Pyramid by observation of cosmic-ray muons, *Nature*, 21 December 2017, Volume 552, pp. 386–390. DOI:10.1038/nature24647

[123] W.R. Scott, C. Schroeder, J.S. Martin, "An acousto-electromagnetic sensor for locating land mines," *Part of the SPIE Conference on Detection and Remediation Technologies for Mines and Minelike Targets III*. Orlando, Florida, SPIE vol. 3392, 0277-786X, 98, pp. 176-186, April 1998. DOI:10.1117/12.324189

[124] S.I. Ivashov, V.V. Razevig, A.P. Sheyko, I.A. Vasilyev, Detection of Human Breathing and Heartbeat by Remote Radar. Progress in Electromagnetics Research Symposium (PIERS 2004), March 28-31, 2004, Pisa, Italy, pp. 663-666. 68_03.pdf (piers.org)

[125] E. M. Staderini, "UWB radars in medicine," in IEEE Aerospace and Electronic Systems Magazine, vol. 17, no. 1, pp. 13-18, Jan. 2002, DOI: 10.1109/62.978359.

[126] F. Soldovieri, I. Catapano, L. Crocco, L. N. Anishchenko, S. I. Ivashov, A Feasibility Study for Life Signs Monitoring via a Continuous-Wave Radar, International Journal of Antennas and Propagation, Vol. 2012, Article ID 420178, 5 pages, 2012, doi:10.1155/2012/420178.

[127] I. Immoreev, S. Ivashov, "Remote monitoring of human cardiorespiratory system parameters by radar and its applications," 2008 4th International Conference on Ultrawideband and Ultrashort Impulse Signals, Sevastopol, UKraine, 2008, pp. 34-38, doi: 10.1109/UWBUS.2008.4669350.

[128] M.A. Barnes, S. Nag, T. Payment, "Covert situational awareness with handheld ultra-wideband short pulse radar," SPIE Conference on "Radar Sensor Technology VI", Orlando, Fla. 19 April 2001, Proc. SPIE, vol. 4374, pp. 66-77, 2001. DOI: 10.1117/12.438164

[129] Bugaev, A. S., Chapursky, V. V., & Ivashov, S. I. Mathematical simulation of remote detection of human breathing and heartbeat by multifrequency radar on the background of local objects reflections. IEEE International Radar Conference, Arlington, Virginia, USA, May 9-12, 2005, DOI:10.1109/radar.2005.1435851

[130] Marimuthu, J., Bialkowski, K. S., & Abbosh, A. M. (2016). *Software-Defined Radar for Medical Imaging. IEEE Transactions on Microwave Theory and Techniques, 1–10.* doi:10.1109/tmtt.2015.2511013

[131] B. Amin, A. Shahzad, L. Crocco, M. Wang, M. O'Halloran, A González-Suárez, M. Elahi, A feasibility study on microwave imaging of bone for osteoporosis monitoring. Med Biol Eng Comput (2021). doi: 10.1007/s11517-021-02344-8

[132] M. T. Bevacqua, S. Di Meo, L. Crocco, T. Isernia and M. Pasian, "MILLIMETER-WAVES BREAST CANCER IMAGING VIA INVERSE SCATTERING TECHNIQUES," in IEEE Journal of Electromagnetics, RF and Microwaves in Medicine and Biology, DOI: 10.1109/JERM.2021.3052096

[133] L.N. Anishchenko, A.A. Demendeev, S.I. Ivashov, V.V. Razevig, I.A. Vasiliev, T.D. Bechtel. Holographic Radar in Breast Cancer Imaging, RADARCON 2012, Atlanta, USA, 2012. pp. 1004-1007. DOI:10.1109/radar.2012.6212284

[134] Cuccaro, A.; Dell'Aversano, A.; Ruvio, G.; Browne, J.; Solimene, R. Incoherent Radar Imaging for Breast Cancer Detection and Experimental Validation against 3D Multimodal Breast Phantoms. *J. Imaging* **2021**, *7*, 23. https://doi.org/10.3390/jimaging70200233

[135] Semenov, S. Y., & Corfield, D. R. (2008). *Microwave Tomography for Brain Imaging: Feasibility Assessment for Stroke Detection. International Journal of Antennas and Propagation, 2008, 1–8.* DOI:10.1155/2008/254830

[136] Andrey Zhuravlev, Sergey Ivashov, Vladimir Razevig, Igor Vasiliev, Inverse synthetic aperture radar imaging for concealed object detection on a naturally walking person, Proc. of SPIE Symposium on Defense and Security, Radar Sensor Technology XVIII Conference. Baltimore, Maryland, USA, May 5 – 7, 2014, Vol. 9074, pp. 907402-1…11. DOI: 10.1117/12.2051615

[137] "ProVision® Imaging," 26 March 2014, https://www.leidos.com/sites/g/files/zoouby166/files/2020-07/FS-Leidos-Provision2.pdf

[138] "eqo," 3 June 2013, http://www.smithsdetection.com/index.php/en/products-solutions/people-screening-systems/60-people-screening-systems/eqo.html, (15 January 2015).

[139] Ahmed, S. S. *Personnel screening with advanced multistatic imaging technology. Passive and Active Millimeter-Wave Imaging XVI,* Proc. of SPIE 8715, 2013. DOI:10.1117/12.2018054